Design of Cooling Fins on the Freeze Plug

by

to obtain the degree of

Bachelor of Science in Applied Physics

at Delft University of Technology

Student number:	4306201	
Project duration:	February 10, 2017 – June 10, 2017	
Thesis committee:	Dr. ir. M. Rohde,	TU Delft, supervisor
	Prof. dr. ir. J. L. Kloosterman,	TU Delft

An electronic version of this thesis is available at `http://repository.tudelft.nl/`.

TU Delft

Abstract

Despite the great potential of nuclear reactors, the reputation of nuclear energy in society is damaged. To make a new generation of nuclear reactors successful, improvements on safety and sustainability are of great importance. Accidents in the past have led to a new safety requirement. In the future, nuclear reactors must incorporate a passive protection system. In the Molten Salt Reactor, the passive protection is provided by the freeze plug. The freeze plug is an actively cooled blockage consisting of solidified salt in pipes leading to drainage tanks located underground. In case of a station black out, the plug will melt, enabling the core to flow into underground tanks. To prevent damage to the reactor, this process must be completed within 8 minutes at most.

The aim of this thesis is to investigate whether the current design of the freeze plug can be improved by addition of cooling fins. The cooling fins ensure an efficient heat transfer from the reactor core to the freeze plug and should result in a decrease of the melting time. Research is conducted on the heat transfer properties of various configurations of cooling fins. The heat transfer of the cooling fins is modeled by using an average heat transfer coefficient. Various geometries including an arrangement of cooling fins and a grid of freeze plugs have been tested in COMSOL Multiphysics to discover the most optimal configurations. The results showed a closely packed in-line arrangement of cooling fins resulted in a decrease in melting time of around 40 seconds, reducing the total melting time by approximately 25%. Based on the research, it can be concluded that adding cooling fins to the current design of the freeze plug is useful.

Contents

List of Figures

List of Tables

Nomenclature

Symbol	Description	Units
Δ	shortest distance between edges of the cooling fin and the freeze plug	m
λ	thermal conductivity	$\mathrm{W m^{-1} K^{-1}}$
$\langle k \rangle_{fin}$	average heat transfer coefficient for a cooling fin	$\mathrm{W m^{-2} K^{-1}}$
$\langle k \rangle_{top}$	average heat transfer coefficient for a flat plate	$\mathrm{W m^{-2} K^{-1}}$
$\langle Nu \rangle_{fin}$	average Nusselt number for a cooling fin	-
$\langle Nu \rangle_{top}$	average Nusselt number for a flat plate	-
μ	dynamic viscosity	$\mathrm{kg m^{-1} s}$
ν	kinematic viscosity	$\mathrm{m^2 s^{-1}}$
ϕ''	heat flux density	$\mathrm{W m^{-2}}$
ρ	density	$\mathrm{kg m^{-3}}$
ζ_L	dimensionless longitudinal pitch	-
ζ_T	dimensionless transversal pitch	-
a	thermal diffusivity	$\mathrm{m^2 s^{-1}}$
D	characteristic diameter	m
D_{fin}	diameter of cooling fin	m
D_{plug}	diameter of freeze plug	m
h_{fin}	height of cooling fin	m
h_{plug}	height of freeze plug	m
k	heat transfer coefficient	$\mathrm{W m^{-2} K^{-1}}$
N	amount of tubes in the tube bank	-
Nu	Nusselt number	-
Nu_D	Nusselt number based on tube diameter	-
Nu_x	Nusselt number based on the x-position	-
P	distance between adjacent freeze plugs	m
PDR	ratio of P and D_{plug}	-
Pr	Prandtl number	-
R_{fin}	radius of cooling fin	m
R_{plug}	radius of freeze plug	m
Re	Reynolds number	-

Re_D	Reynolds number based on tube diameter	-
Re_x	Reynolds number based on the x-position	-
S_D	diagonal distance between two consecutive tubes	m
S_L	longitudinal distance between two consecutive tubes	m
S_T	transversal distance between two consecutive tubes	m
T	temperature	K
t	time	s
T_0	Initial temperature	K
T_∞	temperature of environment	K
t_{melt}	melting time	s
T_s	temperature of the surface	K
U_{app}	applied velocity	$\mathrm{m\,s^{-1}}$
U_{max}	maximum velocity in tube bank	$\mathrm{m\,s^{-1}}$
v	flow velocity	$\mathrm{m\,s^{-1}}$

1 Introduction

The energy transition is imminent, a structural change in energy systems is required to tackle climate change which involves a reduction in the dependency on fossil energy sources. Alternative energy sources consist of renewables and nuclear energy. Extensive research on the optimisation of these energy sources has led to great technological improvements. Amongst others, nuclear energy proved to be a promising energy source. However, in the fields of safety, nuclear waste and sustainability improvements are essential. Nuclear waste is dangerous for most forms of life and the environment and remains dangerous for a long time. Not only great amounts of nuclear waste have to be stored for this period, but also the enormous time span makes it difficult to communicate the storage locations to generations thousands of years ahead. Besides, due to major accidents in the past with nuclear power plants, the reputation of nuclear energy in society is damaged. To make a new generation of power plants successful, improvements on safety and sustainability are of great importance. An organisation dealing with the development of these generation IV reactors is named GIF (Generation IV International Forum). GIF selected six technologies for further research and development [3]. These include:

- Gas-cooled Fast Reactor (GFR)
- Lead-cooled Fast Reactor (LFR)
- Molten Salt Reactor (MSR)
- Supercritical Water-cooled Reactor (SCWR)
- Sodium-cooled Fast Reactor (SFR)
- Very High Temperature Reactor (VHTR)

Delft University of Technology contributes to the research and development of the Molten Salt Fast Reactor by participating in the SAMOFAR project. A project consortium that consists of eleven partners including Delft University and has its focus on innovative safety systems and optimal waste management of the Molten Salt Fast Reactor. One of the innovative safety systems in the MSFR is the freeze plug, which will be the focus of this thesis.

1.1. Molten Salt Fast Reactor

Molten Salt Reactors (MSR) is a class of nuclear fission reactors. One specific reactor in this class is the Molten Salt Fast Reactor (MSFR). In these reactors the primary coolant is a molten salt mixture in which the fissile material is dissolved. As coolant, fluoride salts are often used. The liquid fuelled MSFRs can operate using any fissile material, but the MSFR is often associated with the ^{233}U – ^{232}Th fuel cycle which results in significantly less generation of highly radiotoxic elements and a higher fuel burn-up compared to the conventional uranium reactors. The physical properties of the salt enable a MSFR to operate at high temperatures (up to 750°C) and at nearly atmospheric pressure. In the core, fission occurs within the fuel salt. The heated mixture flows to a heat exchanger where a part of the heat is transferred to a secondary salt coolant used to generate electricity. Hereafter, the fuel salt flows back to the core. In the reactor, another fluid circuit continuously

extracts the fission products and introduces new fertile material into the fuel salt. There is a closed flow of molten salt through the reactor along heat and fissile products are extracted and fertile material is introduced. A schematic overview of the Molten Salt Fast reactor is shown in figure 1.1.

The fluid-fuel system has beneficial safety characteristics. The liquid substance has a high coefficient of thermal expansion which ensures that in the case of overheating, the molten salt expands and reduces the rate of nuclear reactions and thus making the reactor self-regulating [11]. In case of failure, the chain reaction of the fissions can be interrupted but the fissile products continue to produce heat by radioactive decay. The produced heat must be extracted actively otherwise it may cause the reactor to overheat. To illustrate the possible consequences of overheating, a sidestep to the Fukushima disaster in 2011 is made.

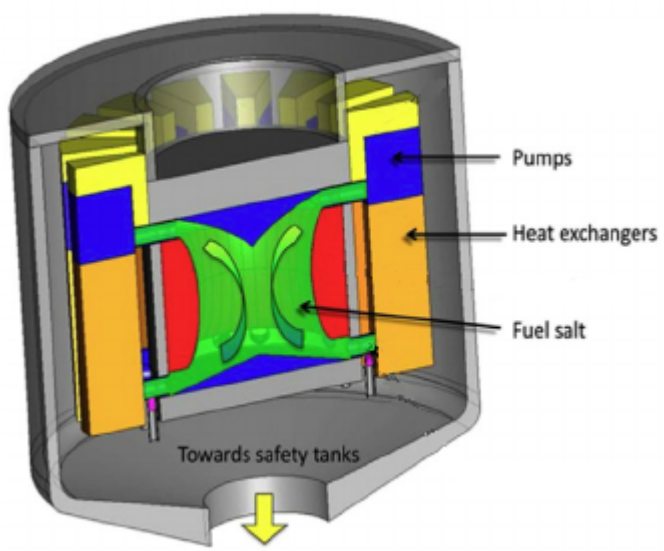

Figure 1.1: Schematic overview of a Molten Salt Fast Reactor [11].

1.2. The Fukushima accident

In March 2011, an earthquake occurred with its epicentre 160 kilometers away from Fukushima. In Fukushima six operating Boiling Water Reactors were located. As a consequence of the earthquake, the reactors were separated from external power sources and operations were terminated. The reactor cores continued to produce heat due to the radioactive decay of fission products. To remove the residual heat, back-up generators were started to take over the cooling of the cores. The earthquake initiated a tsunami, 5 meter higher than the plants were designed for, arriving at the coast 50 minutes later [8]. The tsunami flooded the back-up generators leading to the shutdown of the generators and ultimately of the cooling systems. At this moment, the stations were completely isolated and due to the lack of cooling the station suffered a nuclear meltdown.

The accident has led to an important safety requirement for future reactors. The fourth generation of reactors must incorporate a safety system that makes the reactor inherently safe. The safety systems may no longer be dependent on for example external power sources and back-up generators but should be able to bring the reactor passively in a stable state. The system providing the passive protection in the MSFR is called the freeze plug.

1.3. The freeze plug

The freeze plug is a blockage consisting of solidified salt in pipes leading to drainage tanks located underground. The plug is cooled actively by a cooling system. In case of a black out of the cooling mechanisms responsible for cooling during normal operation of the reactor, the reactor core will start to heat up. Since the cooling of the freeze plug will black out as well, the freeze plug starts to melt under influence of the temperature of the reactor core. Eventually, the freeze plug will melt, opening the pipe to the drainage tanks. The liquid fuel salt flows into the drainage tanks where it can be held under safe conditions during the time of emergency and thus bringing the reactor passively into a stable state.

To ensure a proper operation of the freeze plug, the reactor must be drained before the reactor core

is damaged by the increasing temperature. In normal conditions the reactor operates at a temperature of around 700°C. The maximum temperature the reactor core can sustain is 1200°C which is reached in 8 minutes after terminating the operations of the reactor [1]. The melting process of the freeze plug and the drainage process must be completed within this time interval. In order to do so, the freeze plug must be optimised in terms of a minimal combination of melting time and draining time.

1.4. Previous research

The original design of the freeze plug was a single plug blocking the whole pipe which was studied by Swaroop [12]. A simplified 1D analytical model was constructed to research the melting behaviour of the plug when heating only occurs at the top of the plug. Swaroop reported a melting time of 12 minutes for a plug with a depth of 2 cm. To enhance the melting behaviour, a new design was studied by van Tuyll [14] and hereafter by Makkinje [9]. The new design consists of multiple plugs in one pipe. The intermediate space is filled with a metal enabling the heat to approach the plugs from the sides which should lead to a shorter melting time. It can be concluded that the melting time can be decreased to around 45 seconds using freeze plugs with a depth of 3 cm , the draining time is strongly dependent on the plug radius and the pipe radius . In the model used to investigate the performance of the new design of the freeze plug, the heat transfer due to convection that results from the flow in the reactor has not been considered. Instead a perfect heat transfer is assumed between the molten salt and the freeze plug. In this thesis, the heat transfer due to convection is added to the model. Furthermore, cooling fins are added to the design. Expected is that the cooling fins will have a beneficial effect on the heat transfer due to convection.

1.5. Goals and thesis outline

The goal of this thesis is to discover how cooling fins can be integrated in the design of the freeze plug in order to achieve a decrease in the time it takes to melt the freeze plug. It is expected that the heat transfer from the salt to the cooling fins is more efficient than heat transfer from the salt to the top of the freeze plug module. By including cooling fins the surface area and the heat transfer per surface area are increased which could have a beneficial influence on the melting behaviour of the freeze plug. To gain an understanding of the consequences of using cooling fins, the following research questions must be answered:

- Which parameters influence the total heat transfer from the salt in the reactor to the cooling fins?
- How must the values of these parameters be chosen in order to obtain the largest total heat transfer?
- Which parameters have influence on the performance of a configuration of a grid of freeze plugs in combination with a grid of cooling fins?
- How must the values of these parameters be chosen in order to achieve the most optimal configuration in terms of the lowest melting time?
- Which decrease in melting time can be achieved?
- Is the freeze plug design with cooling fins useful?

The structure of this thesis is as follows. First the characteristics of cylindrical cooling fins for different orientations are discussed and a model is proposed to account for the heat transfer due to convection across the cooling fins. Based on these findings in chapter 3 and chapter 4 the melting behaviour is studied using numerical methods in COMSOL Multiphysics for multiple orientations of cooling fins in 2D and 3D. In chapter 5 the results are discussed. Based on the results, the utility of the application of cooling fins in the freeze plug design is discussed in chapter 6.

2

Theory

2.1. Design of the freeze plug module

In this research, the design of the freeze plug module with cooling fins will be studied. To be able to compare the results to a similar design without cooling fins, the design without cooling fins will be studied as well by using the methods of Makkinje [9]. By changing the dimensions of the plugs and the fins, different versions of the designs are obtained. The variables of interest are:

- D_{plug} diameter of the freeze plugs
- D_{fin} diameter of the fins.
- P distance between two adjacent freeze plugs
- S distance between two adjacent cooling fins
- h_{plug} height of the freeze plugs
- h_{fin} height of the fins
- The orientation of the freeze plugs and the fins.

The radius of the freeze plug module is taken to be arbitrary. The amount of freeze plugs that fit in this radius are a result of the values of the parameters above. The shape of the cooling fins is cylindrical and will not be varied in this research. The space between the freeze plug consists of an alloy called Hastelloy N [10]. An overview of the previously described designs and the new design is given in figure 2.1.

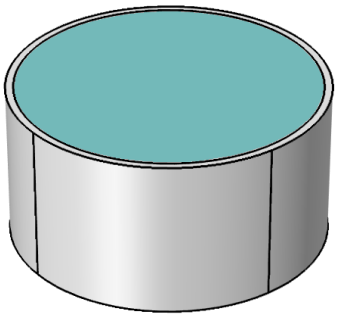

Design consisting of one freeze plug.

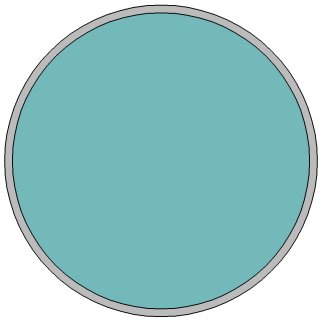

Top view of design consisting of one freeze plug.

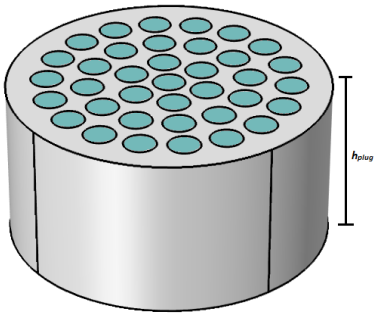

Design consisting of a freeze plug grate.

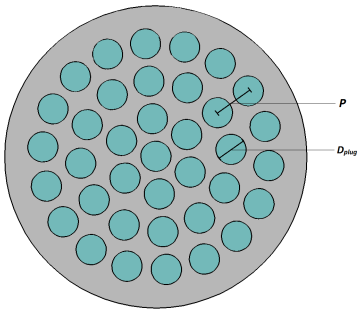

Top view of design consisting of a freeze plug grate.

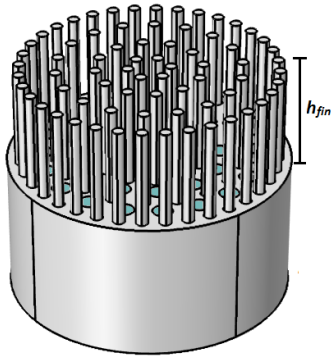

Design including cooling fins.

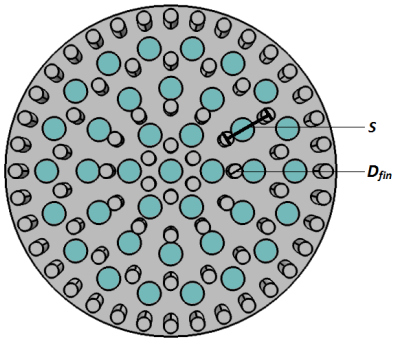

Top view of design including cooling fins.

Figure 2.1: Schematic overview of the previous designs and the new design.

2.2. Heat transfer

The transfer of heat throughout the freeze plug module can be divided into three subclasses.

- Convection
- Conduction
- Radiation

The directions and magnitudes of the heat fluxes in the freeze plug module determine the melting behaviour of the freeze plugs. The melting process of the freeze plugs is based on convection and conduction. Heat transfer due to radiation is negligible and hence neglected.

In case the cooling of the freeze plugs is terminated, a situation arises in which the “hot” molten salt flows over the top of the “cold” uncooled freeze plug module and along the cooling fins. As a result of convection, heat will be transferred from the molten salt to the cooling fins and the top of the freeze plug module. At the top of the freeze plugs a phase change occurs, the frozen salt becomes liquid. Due to convection, the alloy around the freeze plugs and in the cooling fins will be heated. The bottom of the module still has the

"cold" starting temperature and consequently a temperature gradient arises within the alloy. The temperature gradient results in the transport of heat by conduction from the top of the module to the bottom. As the alloy is heating up, it will melt the freeze plugs from the sides (so radially inwards). By the time the sides of the freeze plug at the bottom are melted, the plug will drop under influence of gravity. To be able to describe the heat fluxes, the theory of conduction and convection will be discussed. A schematic overview of the heat fluxes is displayed in figure 2.2.

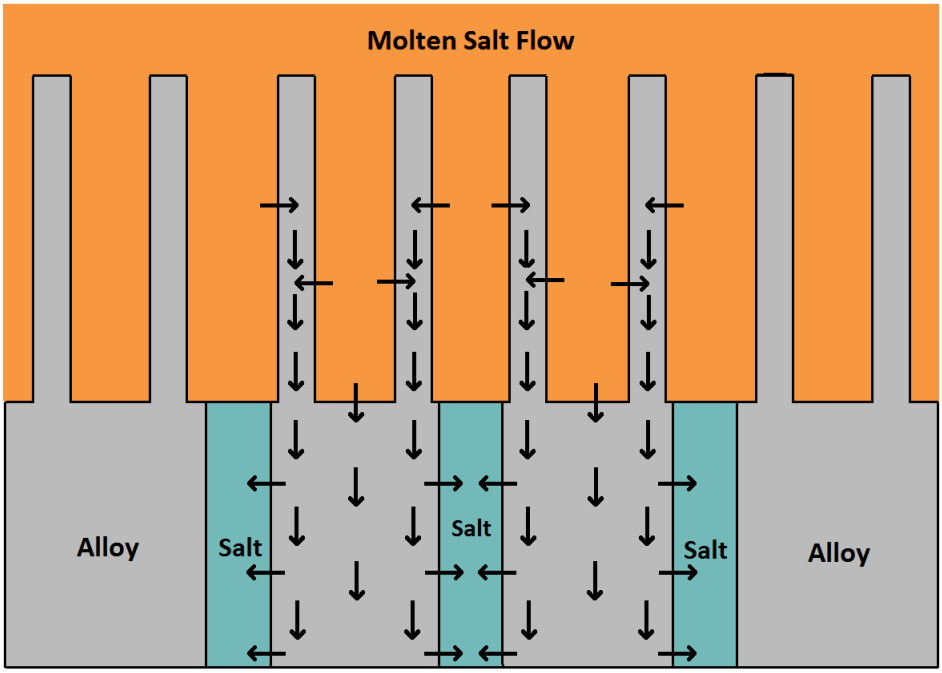

Figure 2.2: Schematic overview of transportation of heat in the freeze plug module. The process is only showed for a part of the module. A heat flux is represented by a black arrow.

2.2.1. Conduction

Conduction stands for the ability of molecules to transport a net amount of heat without transporting mass. Heat transfer by conduction is the dominant factor in the heat transfer within the metal around the freeze plug and in the freeze plug itself. The heat flux that occurs due to a temperature gradient is described by the law of Fourier [13], equation 2.1.

$$\vec{\phi}_q^{"} = -\lambda \nabla T \tag{2.1}$$

According to Fourier's law, a temperature gradient in a particular direction results in a heat flux in this direction in such a way heat is always transferred from a relatively hot area to a cold area. λ represents the thermal conductivity and is a property of a material. It is a measure of the ability of a material to conduct heat. Heat transfer occurs at a higher rate for materials with a high thermal conductivity in comparison to materials with a low thermal conductivity.

2.2.2. Convection

The heat flux caused by convection can be described by Newton's law of cooling [13], equation 2.2.

$$\phi_q^{"} = k(T_\infty - T_s) \tag{2.2}$$

This equation states that the heat flux $\phi_q^{"}$ depends on the difference in temperature of a surface T_s and the temperature of the surroundings T_∞. The parameter k is called the heat transfer coefficient.

When calculating the heat flux through an interface of two media, say A and B, a combination of two heat transfer coefficients is needed. The heat transfer coefficient k_A is a measure of the heat transfer from medium A to the interface. The heat transfer coefficient k_B is a measure of the heat transfer from the surface to medium B. These heat transfer coefficients can be combined in the overall heat transfer coefficient U.

$$\frac{1}{U} = \frac{1}{k_A} + \frac{1}{k_B} \tag{2.3}$$

When medium A is considered to be the molten salt and medium B the alloy, it can be derived that $k_B >> k_A$ thus the overall heat transfer coefficient can be approximated by $U = k_A$. This is equivalent to assuming the temperature of the interface is equal to T_s. To gain a better understanding of where the heat transfer coefficients are related to, the boundary layer theory is discussed.

When a fluid flows past a surface, in the immediate vicinity of the boundary surface, a small layer of fluid is build up where the velocity profile gradually decreases from the velocity of the fluid to zero. Because of the reduced velocity of the fluid, the heat must be transported by conduction through the boundary layer. Since heat transport by convection is more efficient than conduction through the layer, the boundary layer acts as a resistance for heat transport. Therefore, the thermal conductivity and the width of the thermal boundary layer have a major influence on the heat transfer coefficient and is considered to be a direct measure for the resistance of heat transfer across a surface.

The heat transfer coefficient can be transformed into a dimensionless form called the Nusselt number using the following equation.

$$Nu = \frac{kD}{\lambda} \tag{2.4}$$

Here D is the characteristic length scale and λ is the thermal conductivity. The last step in quantifying the heat flux in the stated melting problem is to derive Nusselt relations for the conditions described before. First, two approximations can be made:

1. The interface at the top of the freeze plug can be described as a flat plate in a parallel flow.
2. The cooling fins can be described by an arrangement of cylinders in crossflow.

These assumptions are the starting point of the derivations of appropriate Nusselt relations. The flat plate Nusselt relation is applied to the green boundaries and the Nusselt relation for an arrangement of cylinders is applied to the red boundaries in figure 2.3.

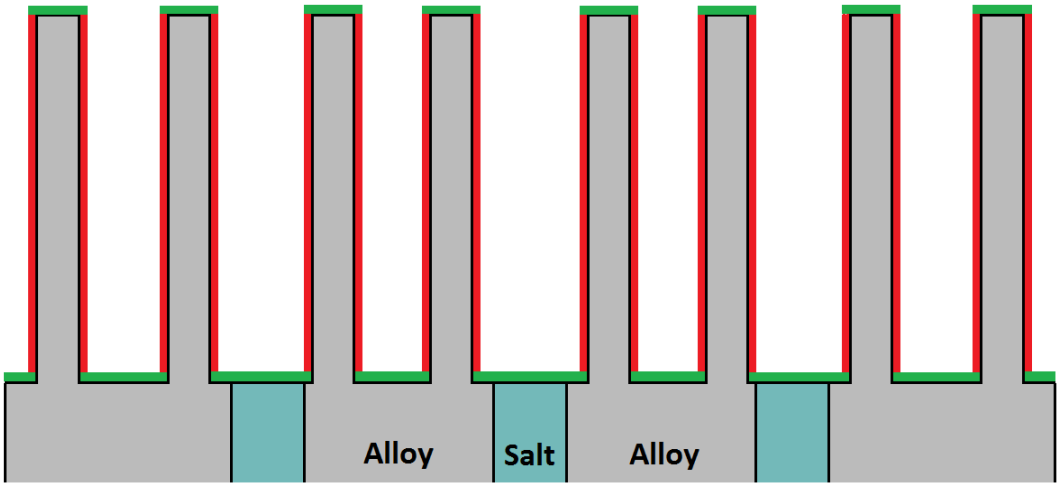

Figure 2.3: Overview of the applied Nusselt relations at the top of the freeze plug module

2.3. Convective heat transfer for a flat plate

Along a flat plate parallel to a fluid flow in say the x-direction, a thermal boundary layer is build up. The width of the thermal layer increases in the x-direction [13]. Therefore, the Nusselt number is dependent on x and is given by equation 2.6.

$$Nu_x = \frac{kx}{\lambda} = 0.332 \cdot \left(\frac{\rho v x}{\mu}\right)^{\frac{1}{2}} \cdot \left(\frac{\nu}{a}\right)^{\frac{1}{3}} \tag{2.5}$$

$$Nu_x = \frac{kx}{\lambda} = 0.332 \cdot (Re_x)^{\frac{1}{2}} \cdot (Pr)^{\frac{1}{3}} \tag{2.6}$$

Equation 2.6 holds for $Re_x < 3 \cdot 10^5$. Here ρ is the density of the fluid, v the velocity of the fluid, x the distance from the starting point of the plate, μ the dynamic viscosity, ν the kinematic viscosity, a the thermal diffusivity, Re the Reynolds number and Pr the Prandtl number. When this relation is integrated over a plate of length L and divided by L, the average Nusselt number is obtained.

$$\langle Nu \rangle = \frac{1}{L}\int_0^L Nu_x dx = 0.221 \cdot \left(\frac{\rho v L}{\mu}\right)^{\frac{1}{2}} \cdot \left(\frac{\nu}{a}\right)^{\frac{1}{3}} \tag{2.7}$$

Equation 2.7 can be used for determining the average Nusselt number at the top of the freeze plug module.

$$\langle Nu \rangle_{top} = \frac{1}{L}\int_0^L Nu_x dx = 0.221 \cdot \left(\frac{\rho v D}{\mu}\right)^{\frac{1}{2}} \cdot \left(\frac{\nu}{a}\right)^{\frac{1}{3}} \tag{2.8}$$

Where D is the lateral characteristic length in the freeze plug module. The average heat transfer coefficient $\langle k \rangle_{top}$ can be calculated using equation 2.9

$$\langle k \rangle_{top} = \langle Nu \rangle_{top} \frac{\lambda}{D} \tag{2.9}$$

2.4. Single cylinder in crossflow

To describe the heat transfer across an arrangement of cylinders, a model of the heat transfer is needed. In this section, first the flow around a single cylinder is discussed qualitatively after which the transition to an arrangement of cylinders is made in the next section.

2.4.1. Flow around single cylinder

The flow of a fluid around a cylinder experiences resistance causing a disturbance of the flow. The characteristics of the flow around and behind the cylinder are dependent on the Reynolds number. Reynolds number is a dimensionless number and is defined by equation 2.10.

$$Re = \frac{\rho v D}{\mu} \tag{2.10}$$

Here D_{fin} is the diameter of the cylinder. Seven flow regimes bounded by Reynolds numbers are distinguished [2]. The exact boundaries may vary from study to study. Since the qualitative behaviour is studied, the stated boundaries suffice here.

(a) Creeping flow $Re < 5$

(b) Attached recirculation zone $5 < Re < 40$

(c) Transitional $40 < Re < 350$

(d) Subcritical $350 < Re < 2 \cdot 10^5$

(e) Critical $2 \cdot 10^5 < Re < 7 \cdot 10^5$

(f) Supercritical $7 \cdot 10^5 < Re < 3.5 \cdot 10^6$

(g) Transcritical $Re > 3.5 \cdot 10^6$

A schematic drawing of the flow around a cylinder for these regimes is displayed in figure 2.4.

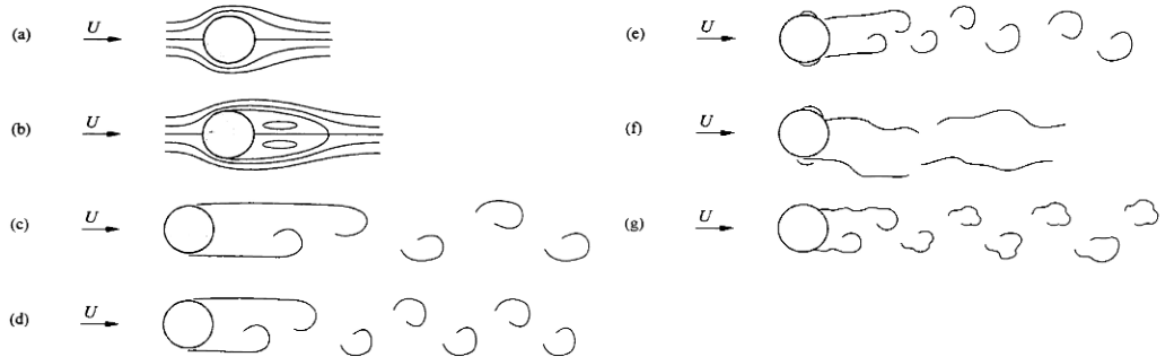

Figure 2.4: The evolution of the flow around a circular cylinder in crossflow for increasing Reynolds number [2].

As can be seen in the figure, the development of the flow around the cylinder can be summarized in the following way.

1. The flow around the cylinder is laminar and no boundary layer separation occurs.

2. The flow starts to separate from the surface and consequently a recirculation zone is formed. As Reynolds increases, the separation point moves downstream. The separation point is the point where the boundary layer separates from the surface of the cylinder.

3. The separation point moves further upstream. Vortex formation and vortex shedding occur in the cylinder wake and the length of the recirculation zone is reduced as Reynolds is increased.

4. The entire flow field of the cylinder may be considered turbulent, except for the boundary layers on its surface. Further changes to the flow field are now influenced by changes in the cylinder boundary layer.

5. The boundary layer undergoes laminar separation followed by turbulent reattachment. The final separation of the boundary layer is now delayed and the cylinder wake becomes increasingly narrow.

The two phenomena that are of particular interest for the heat transfer in an arrangement of cylinders are the character of the wake and the boundary layer separation.

2.4.2. Heat transfer characteristics of a single cylinder

As is observed in the previous section, the surface can be divided into two areas. At various Reynolds numbers the boundary layer on the front area of the tube is laminar. The rear area is in a region of vortex formation. Therefore, one can expect the local heat transfer to be inhomogeneous over the surface of the cylinder. At low Reynolds numbers (up to the transitional regime), the heat transfer in the front area is higher than in the rear area. This can be explained by the existence of the recirculation zone at relatively low values of Reynolds. The fluid in this region is isolated from the bulk fluid and therefore the temperature gradient will decrease at the rear of the cylinder.

As Reynolds increases a shift of the maximum heat transfer coefficient from the front area to the rear area is observed. In the subcritical-critical regime the maximum heat transfer is located at the rear area. This can be explained by the vortex shedding. A vortex shed favours the access of a new hot mass of fluid to the surface and consequently the heat transfer increases suddenly.

In the situation of an arrangement of cylinders, the first array of cylinders will behave similarly as the single cylinder described above. However, the wake of the cylinder extents to multiple times the diameter of the cylinder. For this reason, the flow around the subsequent cylinders placed in this range will be affected by these wakes and thus the heat transfer will be affected as well. The consequences of placing cylinders in a certain arrangement will be studied in the next section.

2.5. Arrangement of cylinders in crossflow

Arrangements of cylinders in crossflow are in scientific research also known as tube banks. Flow conditions in tube banks are dominated by boundary layer separation effects and by wake interactions, which in turn influence the convection heat transfer. These flow conditions are dependent on:

- The orientation of the arrangement.
- The geometrical parameters of the cylinder arrangement.
- The applied fluid flow.

The main interest of this thesis is to understand the effects of the orientation of the arrangement and the geometrical parameters on the heat transfer in a tube bank for a constant applied fluid flow, which is imposed by the operation of the reactor. According to Newton's law of cooling there are three ways to enhance the heat transfer of a tube bank, namely:

- Increasing the heat transfer coefficient.
- Increasing the surface where heat transfer takes place.
- Increasing the temperature difference.

First the average heat transfer coefficient of tube banks will be discussed.

2.5.1. Molten salt flow in the reactor

The flow of the molten salt in the reactor is studied by Frima [4]. In this study the flow path, the flow velocity and the temperature of the molten salt are modeled. The results of the model are displayed in figure 2.5.

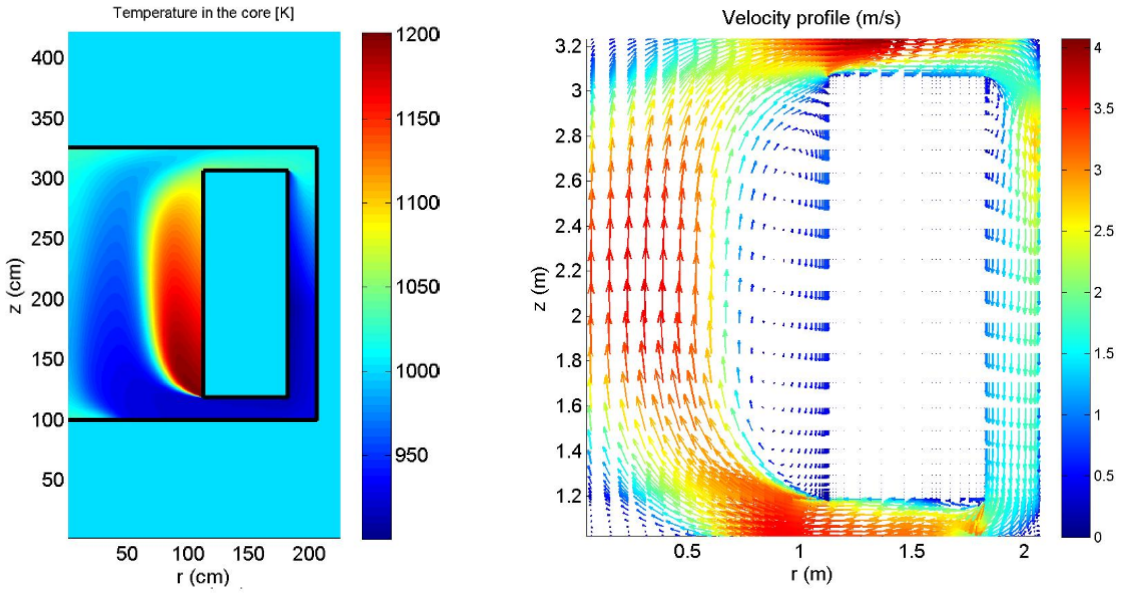

(a) Temperature distribution of the fluid.

(b) Flow velocity and flow path in the reactor.

Figure 2.5: Flow conditions in the core of the reactor. In the left figure the temperature distribution of the molten salt inside the reactor is displayed. In the right figure the flow velocity and the flow direction are showed as a function of position in the reactor [4].

It is assumed the tube bank will be placed at the bottom of the tank (at z = 1m in the figure). Furthermore, it can be derived that the flow will have approximately a velocity of 3.5 meters per second and a temperature of approximately 950 Kelvin. However, in case of a station blackout, the pumps will be shut down and consequently the flow in the reactor will no longer be pumped around. Therefore, the velocity of the flow will gradually decrease over time. An estimation has to be made of the average velocity of the flow entering the tube bank. The average velocity of the flow entering the tube bank is somewhere between 0 and 3.5 meters per second. To ensure a realistic view, a value in the middle of this interval is chosen. The average velocity of

the flow is estimated at 2 meters per second. The applied flow is assumed to be uniform and fully developed at the entry of the tube bank.

In order to further characterize the flow in the reactor the properties of the molten salt must be known. These will be discussed later in this thesis. The applied flow in combination with the geometry of the tube banks will result in Reynolds numbers in the subcritical regime. Therefore, the resulting part of the theory on tube banks will be focused on tube banks in similar conditions.

2.5.2. Geometry of the tube bank

Extensive research has been done on the heat transfer properties of tube banks. A significant amount of the findings is bundled in the books of Zukauskas [15] and Incropera and DeWitt [6]. The findings are mainly based on experiments. To gain a better understanding of the influence of the geometry of a tube bank on the heat transfer capacities in terms of the heat transfer coefficient, the most important findings in the research are discussed. The research was focused on two different orientations, namely the staggered arrangement and the in-line arrangement. An overview of these arrangements is displayed in figures 2.6a and 2.6b.

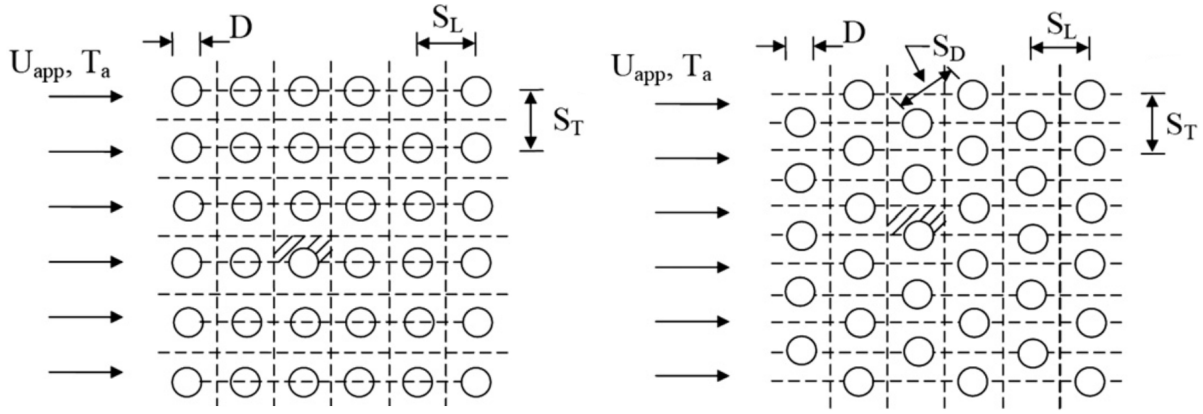

(a) Schematic of in-line arrangement

(b) Schematic of staggered arrangement

Figure 2.6: Schematic overview of the in-line and staggered arrangement. The parameters used to describe the geometry of these types of tube banks are included in the figure. The direction of the applied flow is indicated with the arrows on the left side of the arrangements [7].

The arrangements can be parametrized by defining D_{fin} as the diameter of the cylinders, S_L as the longitudinal pitch, S_T as the transverse pitch and S_D as the diagonal pitch, all measured between the tube's centers. Three dimensionless parameters that are of interest are the dimensionless longitudinal pitch ζ_L, the dimensionless transversal pitch ζ_T and the dimensionless diagonal pitch ζ_D which are given by:

$$\zeta_L = \frac{S_L}{D_{fin}}, \quad \zeta_T = \frac{S_T}{D_{fin}}, \quad \zeta_D = \frac{S_D}{D_{fin}} \tag{2.11}$$

The geometry of the grid affects the flow within the bank and, in general, increases the turbulence in comparison to the undisturbed flow. The turbulence in the tube bank is described by the Reynolds number. The Reynolds number in a tube bank can be calculated using equation 2.12.

$$Re_D = \frac{U_{max} D_{fin}}{\nu} \tag{2.12}$$

Here U_{max} is the mean velocity in the minimum free cross section between the vertical rows of cylinders and can be calculated using equation 2.13 [7].

$$U_{max} = \left(\frac{\zeta_T}{\zeta_T - 1} U_{app}, \frac{\zeta_T}{\zeta_D - 1} U_{app} \right) \tag{2.13}$$

Here U_{app} is the velocity of the applied flow. In banks of both arrangements, flow around a cylinder in the first row is similar to flow around a single cylinder, but the flow pattern in subsequent rows is different due to the disturbance by the previous rows of cylinders. In fact, the tubes of the first few rows act as a turbulence

generating grid after which it is observed that flow conditions stabilize such that little change occurs in the convection coefficient for a tube beyond the fourth or fifth row.

The characteristics of the flow and the amount of turbulence in the tube bank are highly dependent on the dimensionless pitch parameters defined in equation 2.11. By reducing the dimensionless transversal pitch, a nozzle effect is created and the velocity of the flow between the cylinders is increased and consequently the turbulence in the tube bank. When the dimensionless transversal pitch is increased the velocity of the flow between the cylinders will approach the velocity of the applied flow. Furthermore, for relatively large values of ζ_T the cylinders in a vertical row are not influencing each other anymore. As a consequence of this, the staggered arrangement becomes closely similar to the in-line arrangement.

By changing the dimensionless longitudinal pitch, the distance between two cylinders in a horizontal row can be adjusted. By discussing two extreme cases of the dimensionless longitudinal pitch, insight is gained in how this affects the flow in the tube bank. For a tiny dimensionless longitudinal pitch, the flow is closely similar to a flow in a channel. For an infinite dimensionless longitudinal pitch, it results in a flow through a single transverse row, with the velocity profile of the flow behind the preceding row being straightened. In the intermediate cases, the cylinders are located in the wake of the inner rows and the flow preceding one of the inner rows is vortical with a nonuniform velocity distribution.

At last, a comparison between flow through an in-line bank and a staggered bank is made. Flow in an in-line bank is often comparable with that in a straight channel. In staggered banks the flow is comparable with flow in a curved channel of periodically converging and diverging cross section. So, the path of the main flow is more tortuous and a greater portion of the surface area of downstream tubes remains in this path. In general, heat transfer enhancement is favoured by the more tortuous flow of a staggered arrangement.

2.5.3. Heat transfer efficiency for various tube banks

The heat transfer coefficient from the surface of a tube bank to its surroundings is defined by a Nusselt number and the diameter of the tubes. Due to the flow conditions around a cylinder in a tube bank, the heat transfer across the surface is not uniform. To describe the heat transfer from the fluid to the cylinder in an efficient way, an average of the heat transfer coefficient of the surface can be used. This can be achieved by using an average Nusselt number. The Nusselt number is averaged over the surface of the cylinder, excluding the tip, and over all the cylinders in the tube bank. This implies that a cylinder in the first row is considered to have the same heat transfer coefficient as a cylinder in downstream rows. Zukauskas proposes the following form of the Nusselt relation for a cylinder in a tube bank:

$$\langle Nu_D \rangle = C \cdot Re_D^m \cdot f(Pr) \tag{2.14}$$

This Nusselt relation can be used to calculate the heat transfer coefficient using equation 2.4. It can be derived that the average Nusselt number depends on a correction factor C, compensating for the overall geometry of the tube bank. Furthermore, the Nusselt number depends on Re_D to the power m. Here m depends on the geometry of the tube bank as well. Finally, it depends on the Prandtl number. The Prandtl number is assumed to be constant and is a property of the molten salt. The Prandtl number can be computed using equation 2.15.

$$Pr = \frac{\mu C_p}{\lambda} \tag{2.15}$$

Research has been done on the behaviour of $\langle Nu_D \rangle$ for tube banks by varying the dimensionless pitches for both the in-line arrangement and the staggered arrangement. First, the in-line arrangement is discussed. The results of this research are shown in figure 2.7. It must be noted that the research is conducted for flows in the subcritical and critical regime.

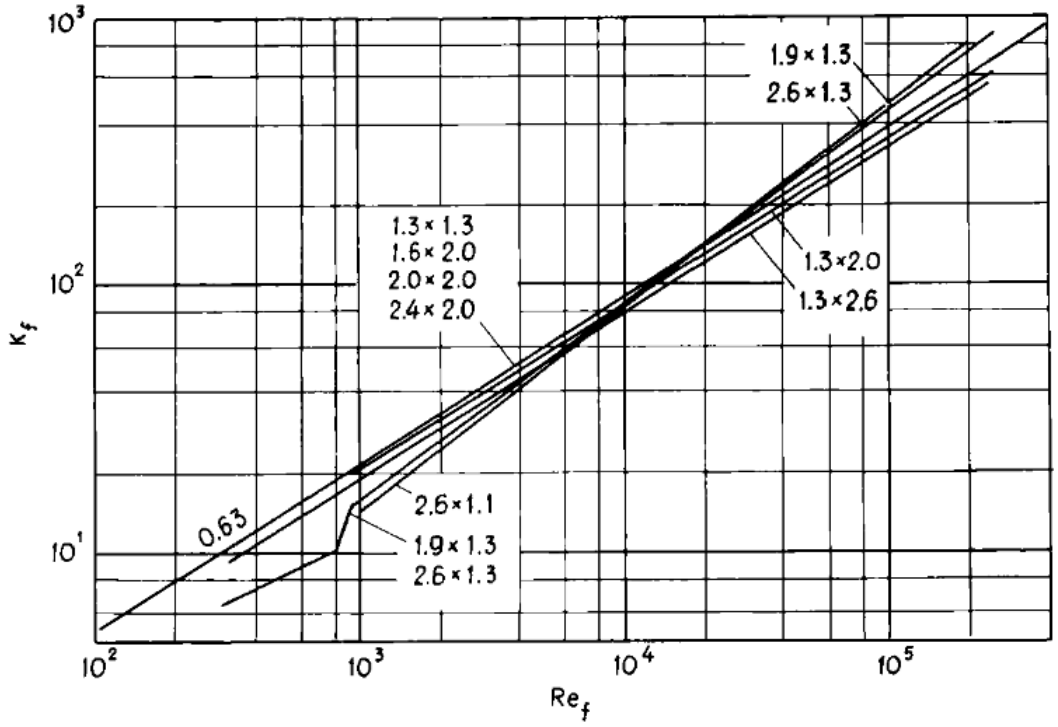

Figure 2.7: Plot of the Reynolds number in the tube bank versus the heat transfer for in-line tube banks with various geometries. The heat transfer is expressed in terms of K_f, where $K_f = CRe_D^m$. For every tested geometry a line is added in the graph and labeled with ζ_T x ζ_L [15].

The figure shows a comparison for 11 various banks of in-line arrangements. The slope of the plots is varying for the compared banks. It can be concluded that an increase of m is observed for constant longitudinal and decreasing transversal pitch. For the stated range of Reynolds numbers, tube banks with relatively low longitudinal pitch perform better than tube banks with relatively large longitudinal pitch. Besides, for flows in

the subcritical regime and closely spaced tube banks a decrease in the transversal pitch leads to an increase of the heat transfer, this dependence is not observed for more widely spaced tube banks. For flows in the critical regime, a small increase in the heat transfer is observed for increasing transverse pitch.

The results of the research on staggered banks are displayed in figure 2.8.

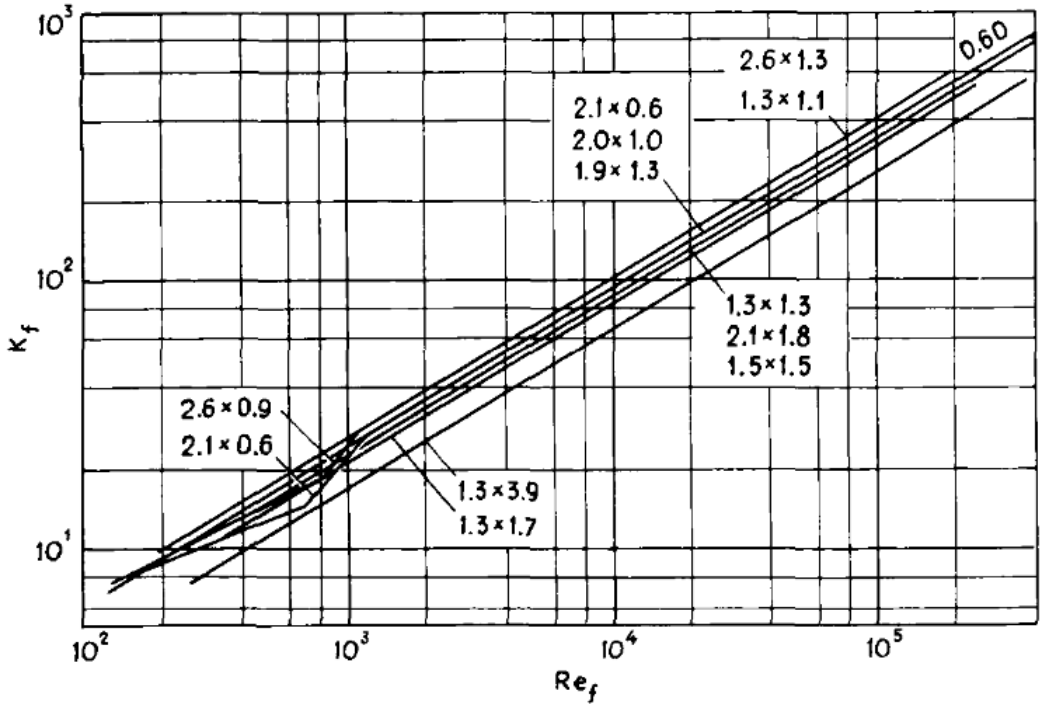

Figure 2.8: Plot of the Reynolds number in the tube bank versus the heat transfer for staggered tube banks with various geometries. The heat transfer is expressed in terms of K_f, where $K_f = CRe_D^m$. For every tested geometry a line is added in the graph and labeled with ζ_T x ζ_L [15].

The figure shows a comparison for 12 various banks of staggered arrangements. Here the effect of the pitch is clear. The power index is the same for all tube banks. However, the heat transfer coefficient increases with a decrease in the longitudinal pitch and, to a lesser extent, with an increase of the transversal pitch. This may be a result of the fact that the flow path becomes more tortuous by increasing the transversal pitch and decreasing the longitudinal pitch. As stated before, this has a beneficial effect on the heat transfer coefficient.

Based on the research, the following can be concluded:

- The heat transfer coefficient of a cylinder in a tube bank is positively influenced by a decreasing longitudinal pitch for both arrangements.
- Increase of the Reynolds number leads to a significant increase in the average heat transfer coefficient of a tube bank and is the dominant parameter for enhancing the heat transfer.
- Increasing the transverse pitch is beneficial for staggered arrangements. However, it should be noted that decreasing of the transverse pitch leads to an increase in the Reynolds number when a constant applied flow is assumed. Since the Reynolds number is the dominant parameter it is likely that this effect will dominate the influence of the transversal pitch.
- Particularly for closely spaced tube banks, staggered arrangements perform better than in-line arrangements.

2.5.4. Modeling the heat transfer coefficient in tube banks: analytical approach

An analytical approach of modeing the convection heat transfer coefficient of tube banks in crossflow has been done by Khan [7]. The resulting analytical model is used in this thesis to predict the average Nusselt

number for a cylinder in a tube bank. Khan came up with the following form of the Nusselt relation:

$$\langle Nu_D \rangle = C \cdot Re_D^{\frac{1}{2}} \cdot Pr^{\frac{1}{3}} \tag{2.16}$$

The determination of the correction factor is done by setting up a model for the hydrodynamic boundary layer that is build up on the surface of a cylinder in the tube bank. For a specific geometry of a tube bank, the correction factor C can be calculated using equation 2.17.

$$C = \begin{cases} [0.25 + e^{-0.55\zeta_L}]\zeta_L^{0.212}\zeta_T^{0.285}, & \text{for in-line arrangement} \\ \frac{0.61\zeta_L^{0.091}\zeta_T^{0.285}}{[1-2e^{-1.09\zeta_L}]}, & \text{for staggered arrangement} \end{cases} \tag{2.17}$$

This equation is valid for $1.05 \leq \zeta_L \leq 3$, $1.05 \leq \zeta_T \leq 3$. The average heat transfer coefficient for a cylinder in the bank can be calculated using equation 2.18.

$$\langle k \rangle = \frac{\langle Nu_D \rangle \lambda}{D_{fin}} \tag{2.18}$$

The influence of the dimensionless longitudinal and dimensionless transverse pitch values on the correction coefficient, implied by the model, for both arrangements are shown in figure 2.9a and figure 2.9b.

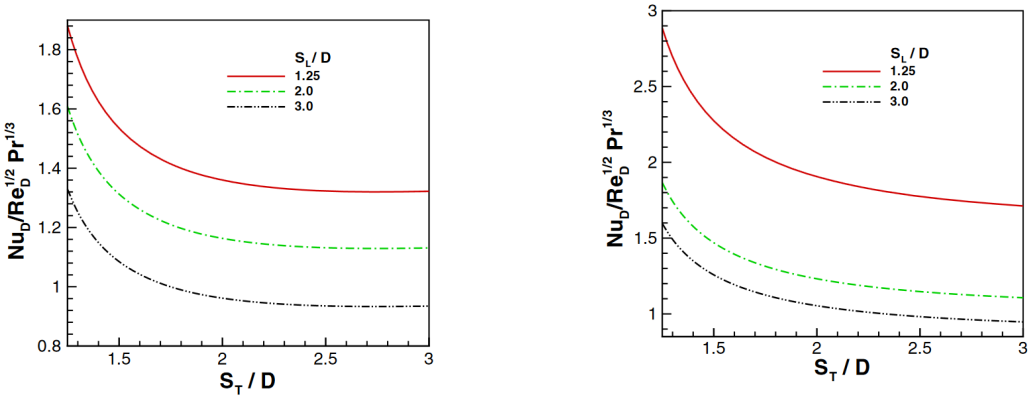

(a) Variation of correction factor for an in-line arrangement.

(b) Variation of correction factor for a staggered arrangement.

Figure 2.9: Variation of correction factor for various ζ_L and ζ_T. On the y-axis the correction factor is displayed and on the x-axis the value of ζ_T. Three plots have been made for three different values of ζ_L [7].

It can be observed that the correction factor increases for a decreasing dimensionless longitudinal pitch and is larger for staggered arrangements than for in-line arrangements. Since the heat transfer coefficient is proportional to the correction factor, a larger correction factor results in a better heat transfer. These results were also found in section 2.5.3. Next, a comparison is made between the heat transfer coefficient for widely spaced staggered and in-line arrangements and for closely spaced staggered and in-line arrangements. The results are shown in figure 2.10a and figure 2.10b.

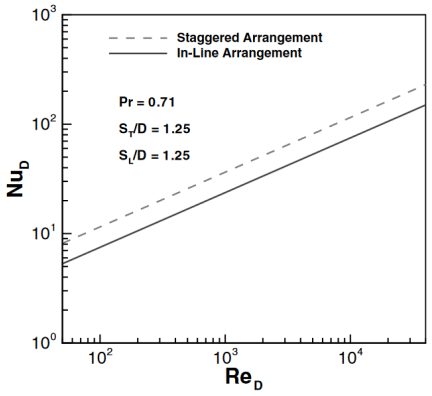

(a) Variation of the average Nusselt number for closely spaced arrangements.

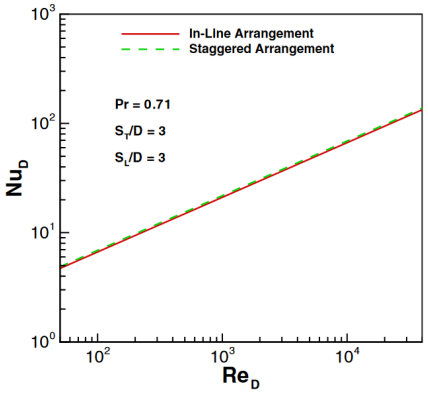

(b) Variation of the average Nusselt number for widely spaced arrangements.

Figure 2.10: Variation of the average Nusselt number for a staggered arrangement and in-line arrangement for ζ_T x ζ_L = 1.25 x 1.25 and a staggered and in-line arrangement for ζ_T x ζ_L = 3 x 3. [7].

Again it can be seen that the plot matches the result from section 2.5.3. For widely spaced arrangements the heat transfer characteristics of a staggered arrangement are similar to those of an in-line arrangement. For closely spaced arrangements the heat transfer coefficient of a staggered arrangement is larger compared to an in-line arrangement.

At last, the values of the model are compared to experimental results obtained by Zukauskas.

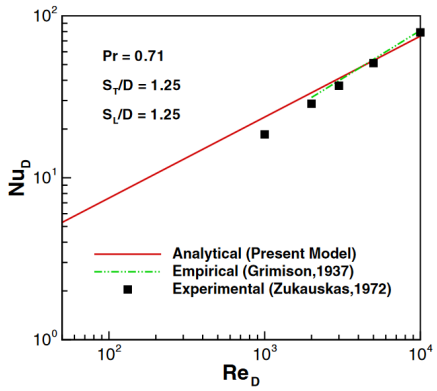

(a) Average Nusselt numbers for a ζ_T x ζ_L = 1.25 x 1.25 in-line arrangement.

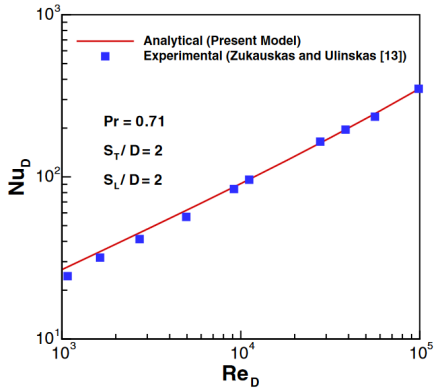

(b) Average Nusselt numbers for a ζ_T x ζ_L = 2 *x* 2 staggered arrangement.

Figure 2.11: Comparison of the average Nusselt number implied by the model to experimentally found numbers. Both an in-line arrangement and a staggered arrangement are compared [7].

The results of the comparison prove that the values following from the model are in good comparison with experimental values for Reynolds numbers in the subcritical regime. However, the model is tested for air flows. In this thesis there must be dealt with a molten salt flow. Zukauskas [15] proved that the heat transfer intensities along the surface of the cylinders are not strongly dependent on the physical properties of the fluid. Fluids with a broad range of Prandtl numbers show similar behaviour along a broad interval of Reynolds numbers. Therefore, the assumption is made that the model is also suited for a flow of molten salt.

2.5.5. Influence of the surface of a tube bank on the heat transfer

The heat transfer rate to the tube bank can be calculated by equation 2.19.

$$Q = kN\pi D_{fin} h_{fin} \Delta T \tag{2.19}$$

Where Q is the heat transfer rate transferred to the tube bank, N is the amount of tubes in the tube bank, h_{fin} is the height of the tubes in the bank and ΔT is the temperature difference between the fins and the bulk of

the flow at a particular moment. For compact tube banks, the amount of cylinders on a surface will increase compared to widely spaced tube banks. As a consequence, the total heat transferred from the environment to the tube bank will increase. As was derived in the previous sections, compact tube banks have in general a higher heat transfer coefficient.

2.5.6. Influence of the temperature gradient in a tube bank on the heat transfer

The previous sections showed that in general compact tube banks are more efficient. However, for very compact banks the assumption that the temperature of the flow in the tube bank is uniform in the flow direction is not valid anymore. When the channels become very small, the temperature of the flow at downstream cylinders is likely to approach the starting temperature of the cylinders. For closely spaced arrangements, the volume of molten salt flowing through the bank is smaller compared to widely spaced arrangements. The total amount of heat in the salt is proportional to the volume of the salt. Therefore, the amount of heat entering the bank is smaller for closely spaced arrangements. For closely spaced arrangements, it is likely that a larger proportion of the amount of heat in the salt is transferred to upstream cylinders. This leads to a stronger decrease of the temperature of the molten salt compared to the decrease that will be observed for widely spaced arrangements. A reduction in the temperature difference between the salt and the surface of the tube bank results in a decrease of the heat transfer rate as can be seen in equation 2.19. On the contrary, in case of a station black-out, the reactor core starts to heat up which may compensate to some extent. In conclusion, to design an efficient tube bank, an optimisation has to be done on a combination of the average heat transfer coefficient, the total surface of the cylinders and the average temperature gradient in the tube bank. In this thesis the assumption is made that the flow has a uniform temperature throughout the tube bank. Therefore, tube banks with dimensionless pitches lower than 1.5 are avoided in the models to ensure a more realistic view. So, in formula:

$$T_\infty(x, y, z) = T_\infty = \text{constant} \tag{2.20}$$

3

Geometries

In the previous chapter the influence of the geometry of tube banks on the heat transfer is examined. In this chapter the knowledge of the tube banks is used to determine how a tube bank can be used to decrease the melting time of the freeze plug in the most efficient way. To achieve this goal, the melting time of various geometries is tested using COMSOL Multiphysics. In this chapter the tested geometries are discussed, the numerical model itself will be discussed in the next chapter.

3.1. Overview of the tested 2-dimensional (2D) geometries

The parameters that may influence the melting time of the freeze plug are:

- $\langle k \rangle_{fin}$ average heat transfer coefficient of the tube bank.
- Δ distance between the edge of the tube with respect to the edge of the freeze plug.
- h_{fin} height of the fins.
- D_{fin} diameter of the fins, equal to two times R_{fin}.
- D_{plug} width of the freeze plug, equal to two times R_{plug}.
- h_{plug} height of the freeze plug.
- P distance between the center of two adjacent freeze plugs.
- PDR ratio of P and D_{plug} .

The models are constructed in such a way the influence of the parameters above on the melting time can be tested. h_{plug} has a major influence on the melting time [9]. When it is increased, the heat has to penetrate deeper into the material. The influence of h_{plug} is beyond the scope of this thesis and is therefore held constant. In order to be able to compare the results with freeze plug modules without cooling fins, first two models without cooling fins are tested. The parametrization of the models is shown in figure 3.1 and 3.2. The freeze plug is displayed in blue and the Hastelloy N in gray.

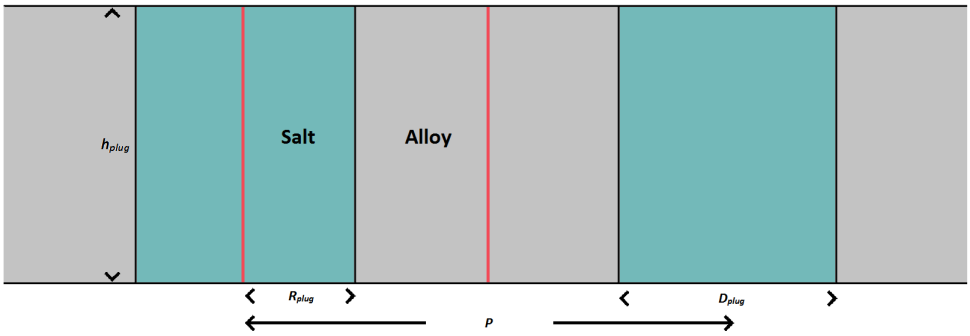

Figure 3.1: Parametrization of the geometries without cooling fins. Due to symmetry reasons, testing the part between the red lines represents the behaviour of an arbitrary amount of freeze plugs in this geometry.

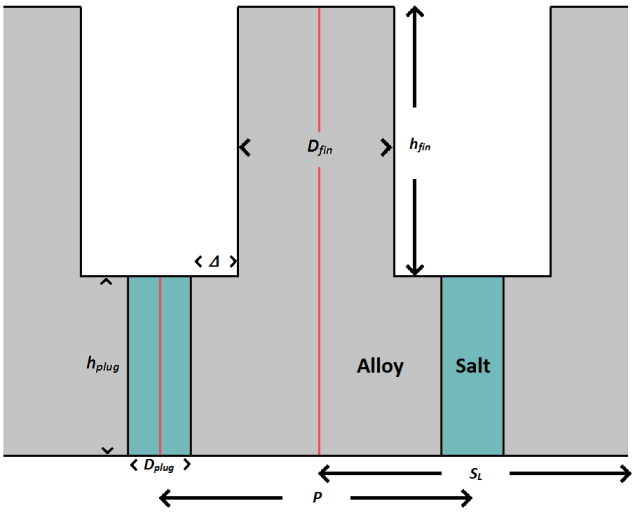

Figure 3.2: Parametrization of the geometries with cooling fins. Due to symmetry reasons, testing the part between the red lines represents the behaviour of an arbitrary amount of freeze plugs in this geometry.

3.1.1. Model 1: Variation of PDR by changing D_{plug}

First a new dimensionless variable is introduced, the PD-Ratio. The PDR can be computed using equation 3.1.

$$PDR = \frac{P}{D_{plug}} \tag{3.1}$$

The influence of D_{plug} on the melting time is examined using the geometry in figure 3.3, where:

- P is held constant.
- D_{plug} ranges from $\frac{1}{5}P$ to close to P.

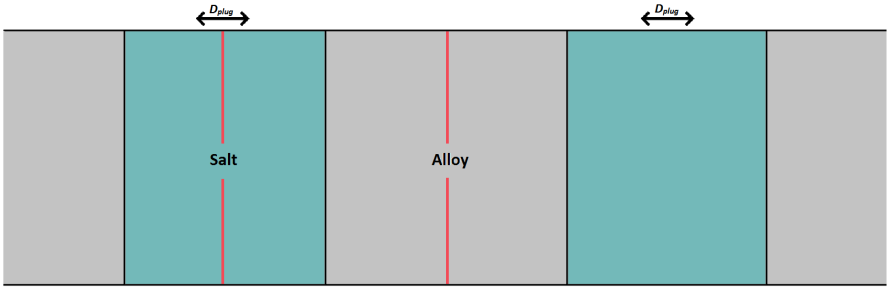

Figure 3.3: Geometry tested in model 1.

3.1.2. Model 2: Variation of PDR by changing P

The influence of P on the melting time is examined using the geometry in figure 3.4, where:

- D_{plug} is held constant.
- P ranges from close to D_{plug} to $5D_{plug}$.

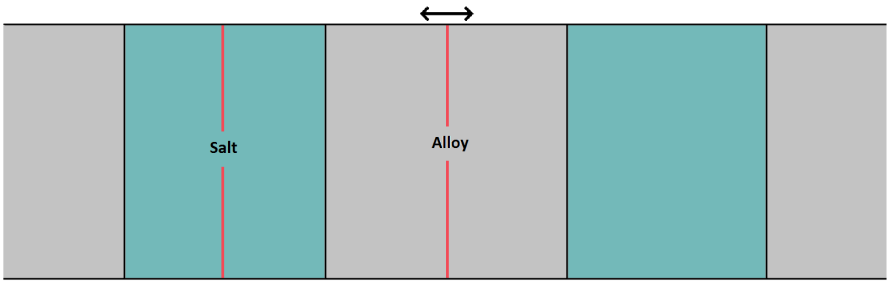

Figure 3.4: Geometry tested in model 2.

3.1.3. Model 3: Variation of Δ

The influence of Δ on the melting time is examined using the geometry in figure 3.5. Δ is the distance between the edge of the cooling fin and the edge of the freeze plug, where:

- ζ_L and D_{fin} are held constant.
- S_L equals P
- D_{plug} ranges from $\frac{1}{10}P$ to $P - D_{fin}$.

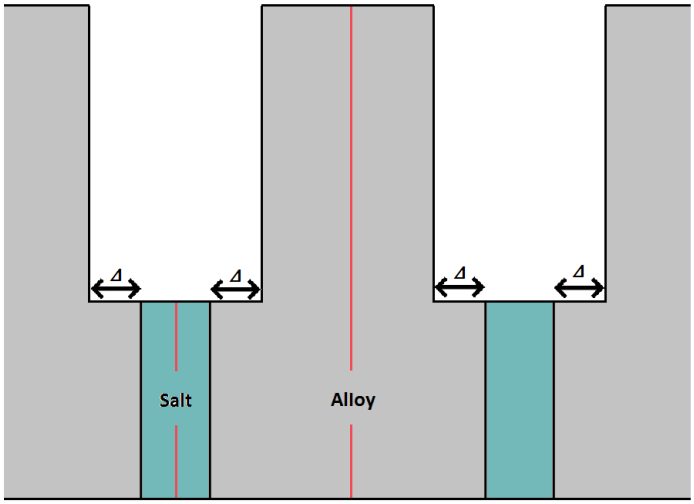

Figure 3.5: Geometry tested in model 3.

3.1.4. Model 4: Variation of h_{fin}

The influence of h_{fin} on the melting time is examined using the geometry in figure 3.6, where:

- S_L and D_{fin} are held constant.
- P and D_{plug} are held constant.
- h_{fin} ranges from D_{fin} to $3D_{fin}$.

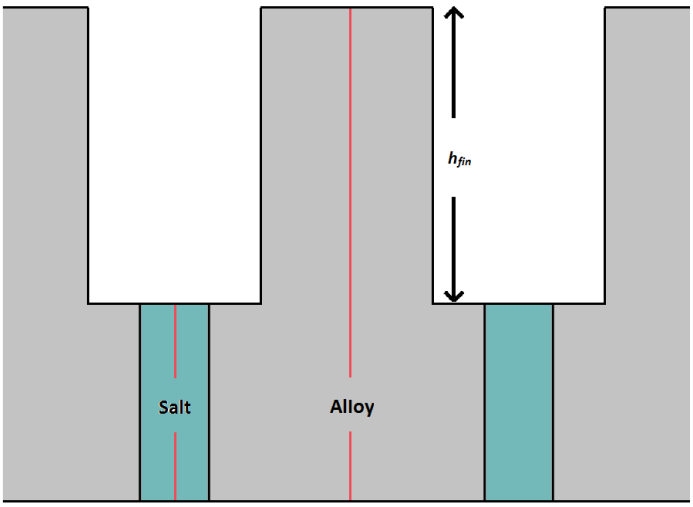

Figure 3.6: Geometry tested in model 4.

3.1.5. Model 5: Variation of D_{fin}

The influence of D_{fin} on the melting time is examined using the geometry in figure 3.7, where:

- S_L and P are held constant and are equal.
- D_{fin} ranges from $\frac{1}{3}S_L$ to $\frac{1}{1.3}S_L$.
- D_{plug} is taken equal to $P - D_{fin} - 2\Delta$, where Δ is taken to be the ideal distance between the edge of a fin and the edge of the plug. This value follows from the result of section 3.1.3.

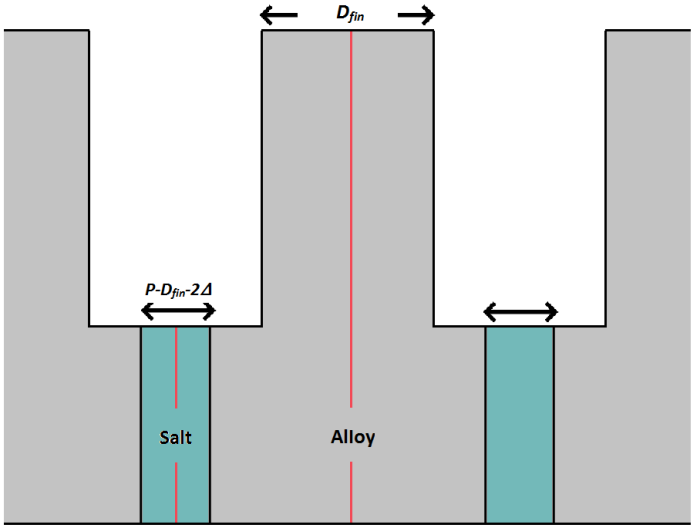

Figure 3.7: Geometry tested in model 5.

3.2. Overview of the tested 3-dimensional (3D) geometries

By combining the obtained theoretical knowledge of tube banks and the results of the models described in section 3.1, 3D geometries are constructed to test the behaviour of the cooling fins in three dimensions. A new parameter that is introduced in 3D are the arrangements of the cylinders and the freeze plugs. Two arrangements are distinguished, the staggered and the in-line arrangement. The integration of the freeze plugs with the cooling fins is done by combining respectively a staggered array and in-line array of cylinders and a staggered array and in-line array of freeze plugs. In this thesis only geometries that satisfy $\zeta_L = \zeta_T$ are tested. The resulting geometries are displayed in figure 3.8a and 3.8b.

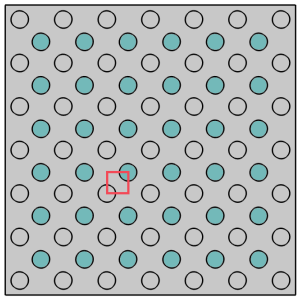

(a) Schematic overview of an in-line arrangement.

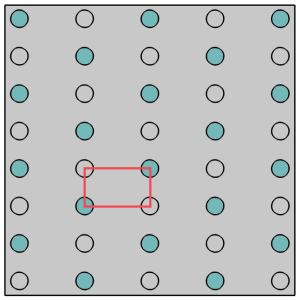

(b) Schematic overview of a staggered arrangement.

Figure 3.8: Overview of the integration of cooling fins and freeze plugs in 3D.

In order to make simple computations in COMSOL possible, symmetry is used. The arrangements are constructed in such a way that a high degree of symmetry is obtained. The unit cells of the arrangements are illustrated with a red rectangular. The results obtained for a computation of the geometry in the unit cell are a representation of the behaviour of the whole geometry. Next, the tested models will be discussed.

3.2.1. Model 6: Variation of PDR by changing P for an in-line arrangement

For the stated scope of this thesis and the geometry of the in-line arrangement, variation of PDR by changing P is similar to variation of ζ by changing S. There is defined:

$$\zeta = \zeta_L = \zeta_T = \frac{S}{D_{fin}}, \qquad S = S_L = S_T \tag{3.2}$$

The influence of the spacing of the arrangement can be tested by varying S, where:

- D_{plug} is held constant and equal to D_{fin}.
- h_{fin} and h_{plug} are held constant.
- ζ ranges from 1.4 to 3.
- PDR ranges from 1.4 to 3.

The tested geometry is displayed in figure 3.9a and 3.9b.

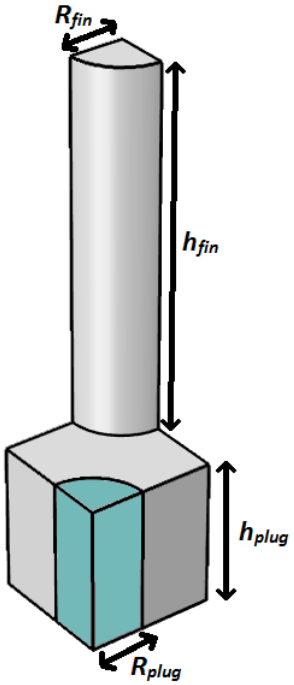

(a) Side view

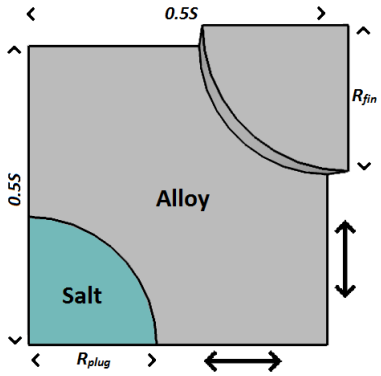

(b) Top view

Figure 3.9: Geometry tested in model 6.

This geometry will be compared to the same geometry excluding the cooling fins. The resulting geometry is displayed in figure 3.10a and 3.10b.

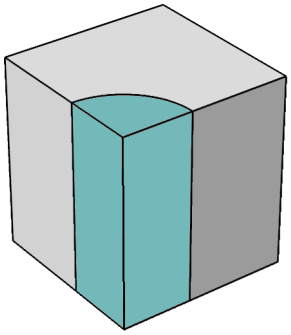

(a) Side view

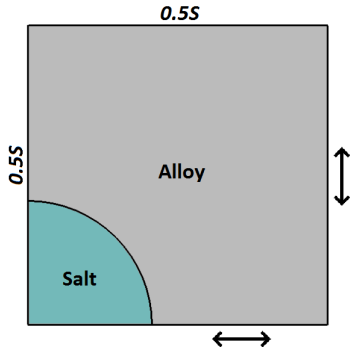

(b) Top view

Figure 3.10: Geometry tested in model 6 without cooling fins.

3.2.2. Model 7: Variation of ζ by changing S for a staggered arrangement

For a staggered arrangement, $\zeta_L = \zeta_T$ results in a geometry with rectangular unit cells. This implies that respectively the horizontal spacing and the vertical spacing between freeze plugs and cylinders in the same row or column are not equal and thus single values of P and PDR in these directions are not defined. However, it can be seen that distances between freeze plugs can be described in exactly the same way as the distances between cylinders. So, for the sake of simplicity this notation will be used for staggered arrangements. This implies that the PDR is here equal to ζ_D. The influence of the spacing of the arrangement for a staggered arrangement is tested in model 7, where:

- D_{plug} is held constant and equal to D_{fin}.
- h_{fin} and h_{plug} are held constant.
- ζ_L and ζ_T range simultaneously from 2 to 3.

The tested geometry is displayed in figure 3.11a and 3.11b.

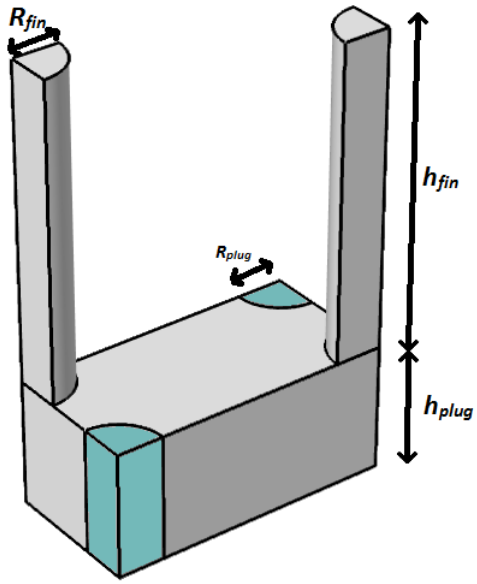

(a) Side view

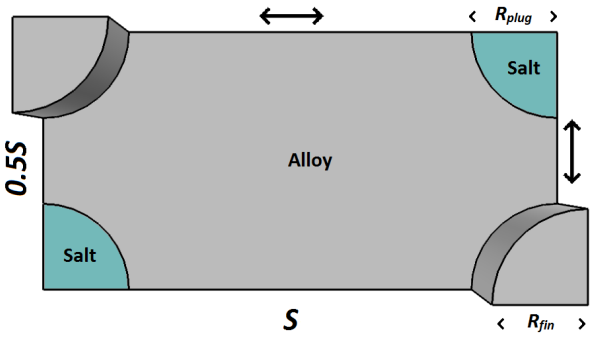

(b) Top view

Figure 3.11: Geometry tested in model 7.

This geometry will be compared to the same geometry excluding the cooling fins. The resulting geometry is displayed in figure 3.12a and 3.12b.

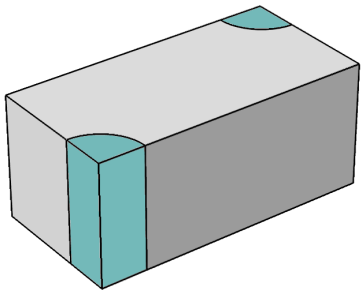

(a) Side view

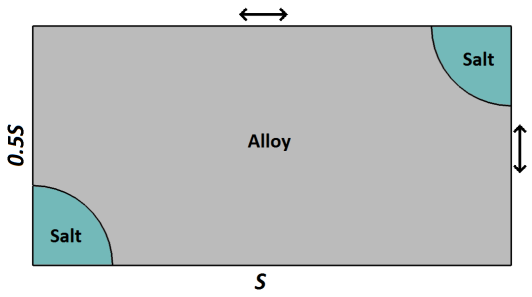

(b) Top view

Figure 3.12: Geometry tested in model 7 without cooling fins.

3.2.3. Model 8: Variation of ζ by changing D_{fin} for an in-line arrangement

This is tested in 3D using model 8. The influence of the diameter of the fin in 3D is investigated in model 8. An in-line arrangement is used because it can be tested for a broader range of ζ values and only a small difference in melting time was observed between staggered arrangements and in-line arrangements. The geometry is tested as follows.

- D_{fin} ranges from $\frac{1}{3}S$ to $\frac{1}{1.4}S$.
- ζ ranges from 1.4 to 3.
- h_{fin} is held constant.
- D_{plug} is held constant.
- PDR is held constant.
- S is held constant.

4

Numerical Methods

The melting process of the freeze plug is modeled in COMSOL Multiphysics. This software can be used to solve physical problems numerically. COMSOL uses finite element methods for the computations. The information needed to simulate the processes in COMSOL are discussed in this chapter.

4.1. COMSOL model for the 2D models

In addition to the geometry, the following information must be specified.

- Materials
- Physics
- Boundary Conditions and Initial Conditions
- Mesh

4.1.1. Materials

Two materials are used for building the geometries, a salt and an alloy. The molten salt flow consists of molten LiF-ThF_4 and the freeze plug consists of solid LiF-ThF_4. Little is known about the physicochemical properties of LiF-ThF_4. Ignatiev [5] investigated the properties of molten LiF-ThF_4 (78 – 22 mol%) for specific temperature ranges. The found properties are displayed in table 4.1. The properties of solid LiF-ThF_4 are unknown. For this reason, for the solid salt the properties of LiCl are used. LiCl is listed in the materials database of COMSOL and is chosen because its melting point is close to that of solid LiF-ThF_4. (610°C for LiCl and 570°C for LiF-ThF_4). Due to this assumption, the computed melting times may be slightly different compared to when the properties of solid LiF-ThF_4 are used. However, it can be expected that the effect of the cooling fins is the same.

Table 4.1: Properties of the molten salt LiF-ThF_4, the temperature T is in K. The value of C_p for 700 °C is extrapolated, since the highest temperature of the validity range is below 700 °C [9].

	Formula	Value at 700 °C	Validity range (°C)
ρ ($g cm^{-3}$)	$4.094 - 8.82 \cdot 10^{-4}(T - 1008)$	4.1249	[620 – 850]
ν ($m^2 s^{-1}$)	$5.54 \cdot 10^{-8} \cdot \exp(3689/T)$	$2.46 \cdot 10^{-6}$	[625 – 846]
μ (Pa s)	ρ ($g cm^{-3}$) $\cdot 5.54 \cdot 10^{-5} \cdot \exp(3689/T)$	$10.1 \cdot 10^{-3}$	[625 – 846]
λ ($W m^{-1} K^{-1}$)	$0.928 + 8.397 \cdot 10^{-5} \cdot T$	1.0097	[618 – 747]
C_p ($J g^{-1} K^{-1}$)	$-1.111 + 0.00278 \cdot T$	1.594	[594 – 634]

The material between the freeze plugs and the cooling fins is Hastelloy N. The choice for Hastelloy N has been made because of its compatibility with Molten Salt Reactors [10]. The physical properties of Hastelloy N are listed in the materials database of COMSOL as well.

4.1.2. Physics, Boundary Conditions and Initial Conditions

The physics package "Heat Transfer in Solids" is used. The heat transfer due to forced convection is modeled by introducing a heat flux across the boundaries in direct contact with the flow. The boundaries are numbered for a geometry with cooling fins and are shown in figure 4.1. The following boundary and initial conditions are taken.

1. Initial Value, T_0=500°C. This value is well below the melting temperature of 570 °C.

2. Thermal Insulation, used for the symmetry axes where the temperature gradient equals zero.

3. Thermal Insulation, it is assumed that heat transfer to the air at the bottom of the freeze plug is negligible. The air at the bottom will be heated when the heat reaches the bottom of the plug. However, a situation arises where hot air is on top of cold air and consequently no natural convection occurs.

4. Heat Flux 1, the magnitude of the heat flux across a flat plate is described by equations 2.1 and 2.9.

5. Heat Flux 2, the magnitude of the heat flux due to forced convection across a tube bank is described by equations 2.1 and 2.18. This condition is only used for the models with cooling fins.

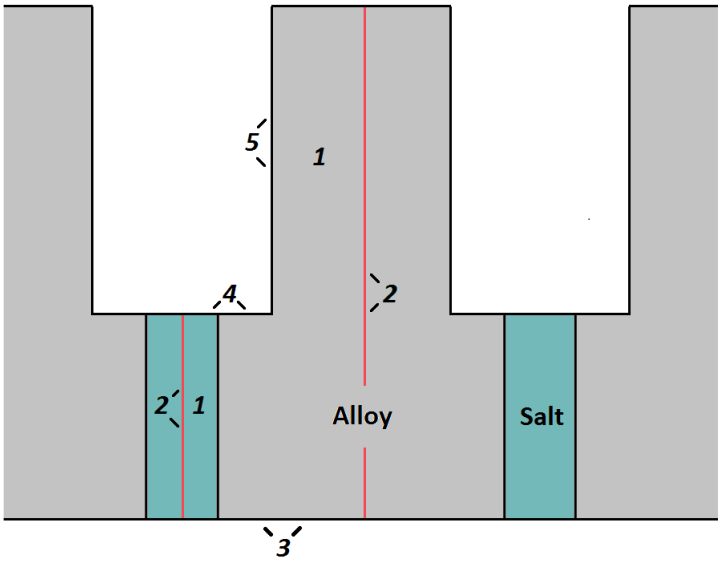

Figure 4.1: Overview of the applied boundary and initial conditions for 2D models. The indicated numbers are matched to the numbers of the enumeration above.

4.1.3. Mesh

Taking care of the mesh is important for obtaining accurate results. An appropriate mesh ensures the results are close to independent on the mesh. Research is done on both the mesh refinement and the mesh type. A more detailed mesh results in more accurate results but has a larger computation time. By using mesh types, distributions can be implemented in the refinement of the mesh. By using an appropriate mesh type, accurate results are obtained for a smaller amount of mesh elements. The two classes of mesh types that are tested are user controlled meshes and a so-called physics controlled mesh. The physics controlled mesh is an option of COMSOL. When this option is selected, COMSOL automatically creates a mesh. A user-controlled mesh enables the user to select the shape of the mesh elements and the distributions of the mesh refinement. Of interest is the melting behaviour at the interface between the frozen salt and the Hastelloy N. Therefore, several distributions in the refinement are introduced near this interface. There will be experimented with the meshes displayed in the figures 4.2a to 4.2d.

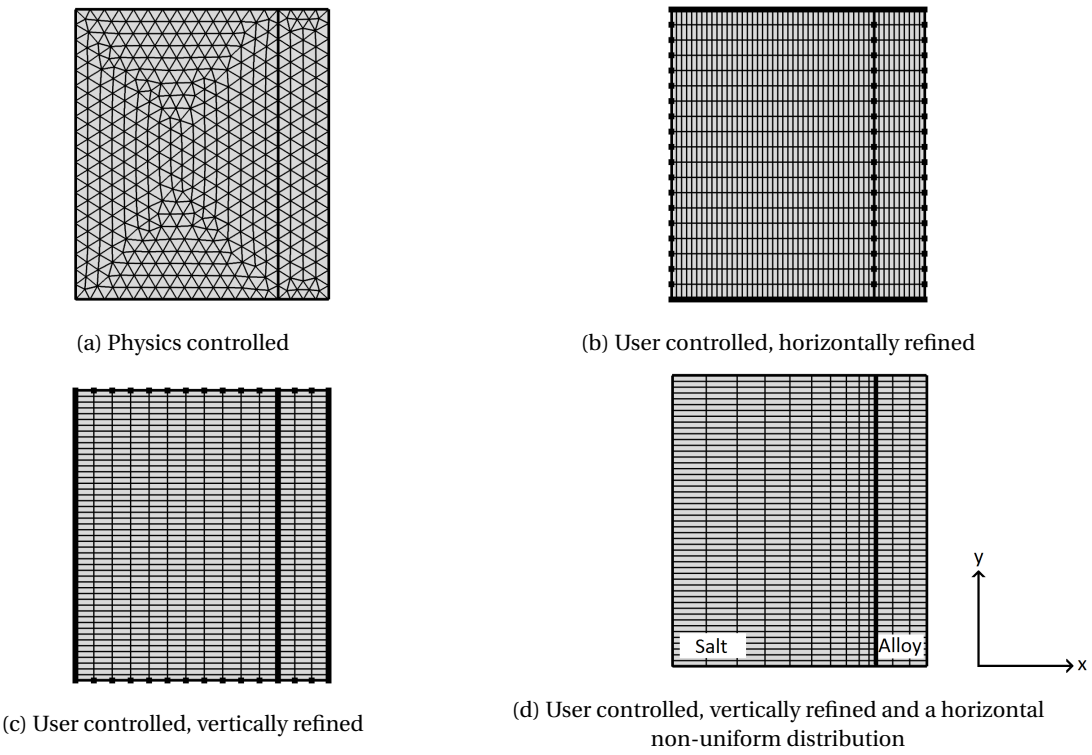

(a) Physics controlled

(b) User controlled, horizontally refined

(c) User controlled, vertically refined

(d) User controlled, vertically refined and a horizontal non-uniform distribution

Figure 4.2: Overview of the different types of meshes that will be tested.

The meshes in figure 4.2a to 4.2d will be tested for various amounts of mesh elements. The mesh type scoring the best on accuracy in combination with the computation time will be used for the models.

4.1.4. Computation of t_{melt}

In COMSOL the function "Line Integration" is used to determine t_{melt}. The interface between the freeze plug and the Hastelloy N is the line over which is integrated. COMSOL stores for every spatial coordinate in the geometry the phase indicator θ_1. θ_1 is defined as:

$$\theta_1(x,y) = \begin{cases} 1, & \text{for solid phase} \\ 0, & \text{for liquid phase} \end{cases} \tag{4.1}$$

This variable is integrated over the interface between the frozen salt and the alloy. The plug has melted over the full length of the edge and consequently drops if the following holds:

$$\int_0^{h_{plug}} \theta_1(R_{plug}, y)\, dy = 0 \tag{4.2}$$

The output of COMSOL is a table with values of the integration for every computed time instance. The melting time is defined as the first time instance at which equation 4.2 holds. To extract the melting time from the table a Matlab script is used. The used script can be found in Appendix A.

4.2. COMSOL model for the 3D models

In general, the 3D models can be processed in COMSOL similar to the 2D models. Only the needed adjustments compared to the 2D models will be discussed. Adjustments are needed in the inputs of:

- Boundary and Initial Conditions
- Mesh
- Computation of t_{melt}

4.2.1. Boundary Conditions and Initial Conditions

The applied boundary conditions and initial conditions for the 3D geometries are:

1. Initial Value 1, T_0=500°C for model 6, model 7 and model 8.1.
2. Initial Value 2, T_0=700°C for model 8.2. This value is used to investigate the effect of the starting temperature of the cooling fins on the melting time of the freeze plug.
3. Thermal Insulation, used for the symmetry axes where the temperature gradient equals zero.
4. Thermal Insulation, it is assumed heat transfer to the air at the bottom of the freeze plug is negligible. The air at the bottom will be heated when the heat reaches the bottom of the plug. However, a situation arises where hot air is on top of cold air and consequently no natural convection occurs.
5. Heat Flux 1, the magnitude of the heat flux across a flat plate is described by equations 2.1 and 2.9.
6. Heat Flux 2, the magnitude of the heat flux due to forced convection across a tube bank is described by equations 2.1 and 2.18. This condition is only used for the geometries with cooling fins.

The boundary conditions are visualised in figure 4.3.

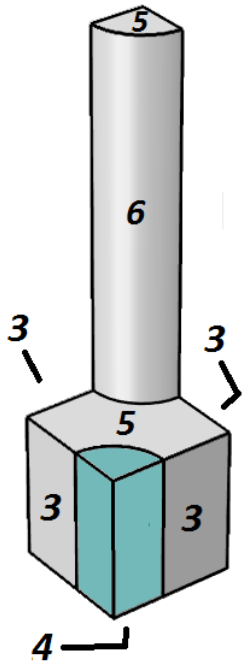

Figure 4.3: Overview of the applied boundary conditions for 3D models. The indicated numbers are matched to the numbers of the enumeration above.

4.2.2. Mesh

The mesh used for the 2D models is not used for the 3D models. The time effort of building a mesh with a similar mesh type in 3D does not compensate for the gain in accuracy for lower amount of mesh elements. Therefore, the more user friendly physics controlled mesh is used. In 2D, a physics controlled mesh consisting of around 1000 elements proved to give a decent balance between computation time and accuracy. This mesh was constructed by making use of the predefined mesh element size settings of a physics controlled mesh and selecting the "normal"/"fine" mesh. To obtain a suitable mesh for the 3D models, a physics controlled mesh is used with the same settings. This will not result in the same amount of mesh elements. However, it is expected that by choosing these settings a decent balance between accuracy and computation time is obtained as well. Besides, it is shown that increasing the amount of mesh elements near the interface of the freeze plug and the Hastelloy N resulted in more accurate results for a shorter computation time. For this reason a "fine" mesh is used in the freeze plug domain and a "coarse" mesh is used in the Hastelloy N domain.

4.2.3. Computation of t_{melt}

t_{melt} is computed in the same way as in the 2D models except the line integration is replaced by a surface integration over the interface between the freeze plug and the Hastelloy N. The phase indicator θ_1 is in 3D defined as in equation 4.3. For the sake of simplicity, cylindrical coordinates are used to describe the surface that is integrated.

$$\theta_1(r,\phi,z) = \begin{cases} 1, & \text{for solid phase} \\ 0, & \text{for liquid phase} \end{cases} \tag{4.3}$$

So, the freeze plug has melted when the following relation holds.

$$\int_0^{h_{plug}} \int_0^{\frac{\pi}{2}} \theta_1(R_{plug},\phi,z) R_{plug} d\phi dz = 0 \tag{4.4}$$

The output of COMSOL is processed with the same MATLAB scripts as was the case for the 2D models.

5 Results

5.1. Mesh refinement

The meshes displayed in section 4.1.3 are tested on model 1. The model is meshed by every type of mesh using in succession approximately 230, 630, 930 and 1300 mesh elements. To observe the influence of the mesh on the melting process, the unmelted length of the freeze plug is plotted against the time. As soon as the unmelted length equals zero, the freeze plug will drop. It can be observed that when the amount of elements increase, the line becomes smoother. Furthermore, a variation in the melting time can be observed when the melting time of a particular geometry is computed for an increasing amount of mesh elements. This effect is clearest for the purple lines. The melting times for meshes with 270 elements and 630 elements are approximately 280 seconds. When the amount of elements is increased to 930, it can be observed that the melting time increases to just over 300 seconds. When the amount of elements is even more increased, the melting time remains at just over 300 seconds. This effect can also observed for the other lines, but to a lesser extent. For a mesh consisting of at least 930 elements, the mesh dependency in the results is strongly decreased. All tested mesh types reach a stable melting time for 930 mesh elements. However, the user controlled mesh with vertical refinement results in the smoothest line for this amount of mesh elements. Therefore, this mesh is considered to be the most optimal mesh from the tested selection and is used for the remaining models. The graphs constructed with this mesh are shown in figure 5.1. An overview of all the graphs can be found in appendix C.

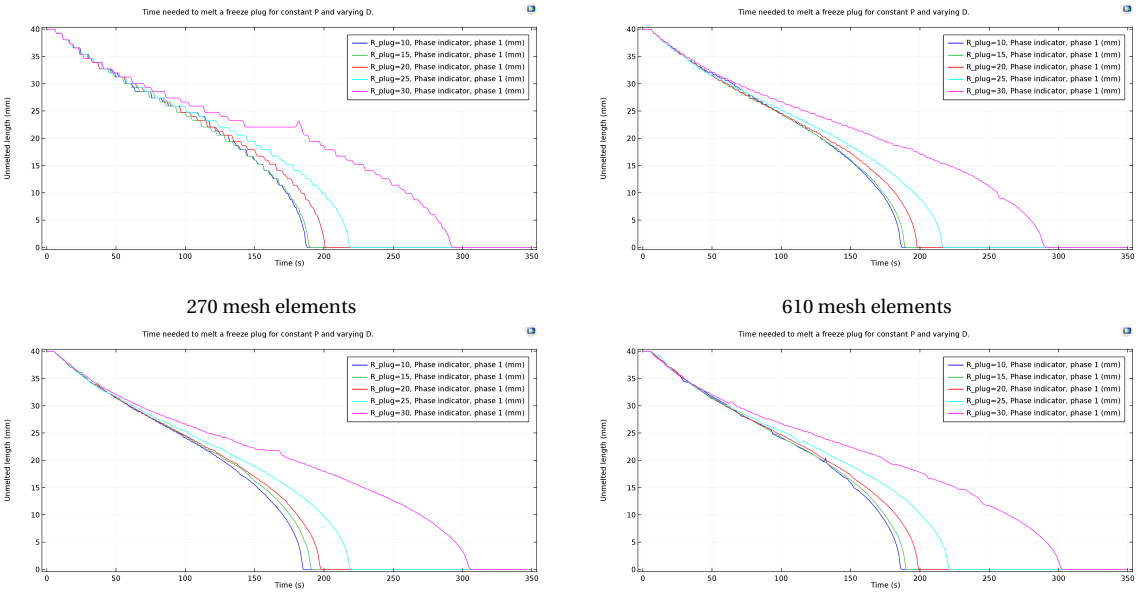

270 mesh elements

610 mesh elements

930 elements

1300 mesh elements

Figure 5.1: Melting time for model 1 using a vertically refined user controlled mesh. P=70 mm.

5.2. Results of the 2D models

Below the results of the 2D models are discussed.

5.2.1. Model 1: Variation of the PDR by varying D_{plug}

In model 1 the diameter of the freeze plug is varied and P is held constant. The minimum height of the plug needed to hold the plug in place is unknown. So, an assumption is needed. The value for h_{plug} is taken to be 40 mm. This height will be held constant for all 2D models. The value of P is taken to be 70 mm. This value is held constant as well for all models except model 2 since in model 2 the influence of P on the melting time is researched. The model is tested for D_{plug} ranging from 14 to 66 mm. These values are chosen since it results in PDR values that are comparable to the work of Makkinje and are in the same order of magnitude as the dimensionless pitch parameters obliged by the model of cooling fins. An overview of the parameter values is shown in table 5.1.

Table 5.1: Overview of the parameter values in model 1.

Parameter	Value	Unit
P	70	mm
h_{plug}	40	mm
D_{plug}	14-66	mm
PDR	1.06-5	-
$\langle k \rangle_{top}$	1465	$\frac{W}{m^2 K}$

The results of model 1 are displayed in figure 5.2. The melting time is plotted as a function of the diameter of the freeze plug, which is in 2D the same as the width of the cooling fin, and as a function of the PDR. The PDR was defined as follows:

$$PDR = \frac{P}{D_{fin}} \tag{5.1}$$

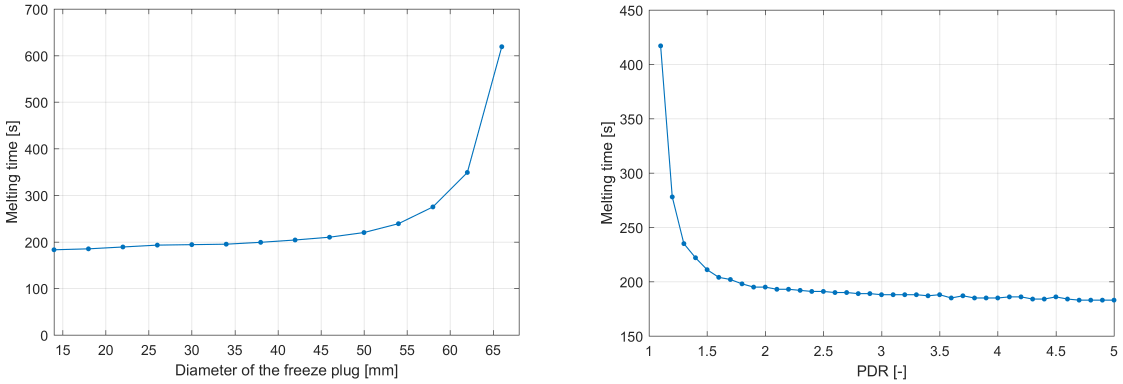

(a) Melting time versus D_{plug}

(b) Plot of the melting time versus the PDR.

Figure 5.2: Plot of the the melting time as a function of the freeze plug diameter and the PDR.

In the figures, it can be seen that for a PDR ranging from 2.5 to 5, the melting time almost remains constant. A fast increase is observed for PDR smaller than 2.5. Since P is held constant, a decrease of PDR is similar to an increase of D_{plug}. Hence a decrease of heat conducting Hastelloy N between the plugs. A conclusion can be made after discussing the results of model 2.

5.2.2. Model 2: Variation of PDR by changing P

In model 2, D_{plug} is held constant at 30 mm. The model is tested for P ranging from 36 to 150 mm. This range for P is taken since it results in the same range of values of the PDR as in model 1. This makes a comparison

possible. An overview of the parameter values is shown in table 5.2 and the results of the model are displayed in figure 5.3.

Table 5.2: Overview of the parameter values in model 2.

Parameter	Value	Unit
P	36-150	mm
h_{plug}	40	mm
D_{plug}	30	mm
PDR	1.2-5	-
$\langle k \rangle_{top}$	1465	$\frac{W}{m^2K}$

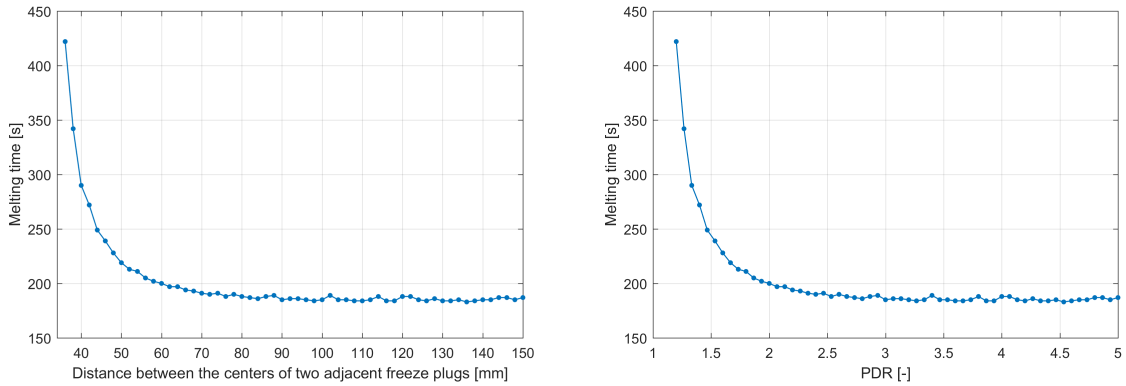

(a) Melting time versus P.

(b) Melting time versus the PDR.

Figure 5.3: Plot of the melting time as a function of the distance between two adjacent plugs.

As can be seen in figure 5.3, the same behaviour is observed as in figure 5.2. An increase of P results in an increase of the PDR. For a PDR larger than 2.5, the melting time remains roughly constant. For a PDR smaller than 2.5 an exponential increase in the melting time is observed. For small values of P, the amount of Hastelloy N between two adjacent freeze plugs will be limited. The total amount of heat flowing into the alloy depends on the width of the interface between the molten salt and the alloy. For a small width of the alloy, the salt-alloy interface is small as well. This results in a reduction of the total amount of heat that can flow into the alloy and therefore, the plug melts slower. If the width of the alloy is increased, the amount of heat flowing into the alloy increases and consequently the freeze plug melts faster. However, when the width of the alloy between the plugs reaches a certain width, the influence vanishes. When the width is increased beyond this certain width, the heat flowing into the alloy at large distances from the edges of the freeze plug will not reach the edges of the freeze plug and therefore, this heat does not contribute to the melting of the freeze plug. Based on conditions and results of model 1 and 2, it can be concluded that there is a minimum amount of alloy equal to 40 mm needed between two freeze plugs to achieve an efficient melting process. The slow decrease of the melting time for a PDR larger than 2.5, as was observed in figure 5.2, is not visible in the results of model 2 and can therefore be addressed to the variation in the diameter of the freeze plug.

It can be concluded that the diameter of the freeze plug has a limited influence on the melting time for values of the PDR larger than 2.5 and P equal to 70 mm. An explanation for this is the following. If the diameter of the freeze plug is increased, the length that has to be melted remains constant and consequently the amount of heat needed to melt the edges. In model 1, the diameter of the freeze plug was varied but P was held constant. Therefore, a decrease in D_{plug} resulted in an increase of the width of the alloy. So, the exponential behaviour observed in figure 5.2 is a consequence of the change in the width of alloy instead of the change of D_{plug}.

5.2.3. Model 3: Variation of Δ

In model 3, cooling fins are included in the geometry. P is fixed at 70 mm. Due to symmetry S_L equals 70 mm as well. As was discovered in chapter 2, a large heat transfer coefficient across the surface of the tubes is achieved by using a closely spaced arrangement of cylinders. This is done by choosing ζ_L=2 and ζ_T=2. These parameters are also taken because the ζ_T x ζ_L=2 x 2 bank is tested on experimental results and the model proved to be in good agreement for these pitches (see figure 2.11b). Since S_L and ζ_L are constant, D_{fin} follows directly from the definition of ζ_L:

$$\zeta_L = \frac{S_L}{D_{fin}} \tag{5.2}$$

$\langle k \rangle_{top}$ and $\langle k \rangle_{fin}$ are computed using the Matlab script displayed in Appendix A. The value of $\langle k \rangle_{top}$ is equal to 1465 $\left[\frac{\mathrm{W}}{\mathrm{m^2K}}\right]$. The value of $\langle k \rangle_{fin}$ is equal to 14275 $\left[\frac{\mathrm{W}}{\mathrm{m^2K}}\right]$.
Δ is defined as follows:

$$\Delta = P - D_{plug} - D_{fin} \tag{5.3}$$

P and D_{fin} are held constant. So, Δ can be varied by varying D_{plug}. D_{plug} ranges from 14 mm to 35 mm and consequently Δ ranges from 0 to 10.5 mm. The stated range for D_{plug} is chosen because it results in PDR values between 2 and 5. This makes a comparison with model 1 possible.

To summarize, $\langle k \rangle_{fin}$ is constant because ζ_L, ζ_T and D_{fin} are constant. The only two parameters that vary are D_{plug} and consequently Δ. The effect of D_{plug} is known from model 1 and 2. Thus, by choosing the parameters in the way described, the effect of Δ can be found. The goal of finding the effect of Δ is to investigate whether the position of the cooling fins with respect to the freeze plugs has effect on the melting behaviour.
An overview of the values of the parameters is shown in table 5.3 and the results are displayed in figure 5.4.

Table 5.3: Overview of the parameter values in model 3.

Parameter	Value	Unit
P	70	mm
h_{plug}	40	mm
D_{plug}	14-34	mm
PDR	2-5	-
S_L	70	mm
h_{fin}	60	mm
D_{fin}	35	mm
ζ_L	2	-
ζ_T	2	-
Δ	0-10.5	mm
$\langle k \rangle_{fin}$	14275	$\frac{\mathrm{W}}{\mathrm{m^2K}}$
$\langle k \rangle_{top}$	1465	$\frac{\mathrm{W}}{\mathrm{m^2K}}$

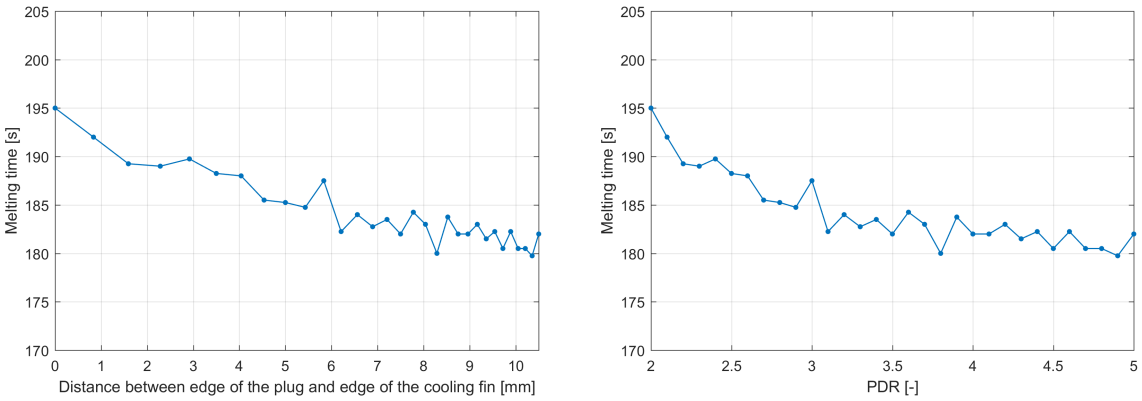

(a) Melting time versus Δ.

(b) Melting time versus the PDR.

Figure 5.4: Plot of the melting time as a function of the distance between the melting edge of the freeze plug and the edge of the cooling fin.

Figure 5.4a and figure 5.4b show that when the cooling fin is placed further away from the freeze plug, the melting time decreases. A possible explanation for this behaviour can be derived by studying a comparison of the results of model 1 and 3. This comparison is made by plotting the lines of figure 5.2b and figure 5.4b in the same figure. In model 3 cooling fins are present, in model 1 cooling fins are absent. Δ is the distance between the edge of a cooling fin and the edge of a freeze plug. However, model 1 has no cooling fins and therefore Δ is not defined. By combining the definitions of Δ and PDR, the following relation between these two parameters is obtained:

$$\Delta = P - \frac{P}{PDR} - D_{fin} = P(1 - \frac{1}{PDR}) - D_{fin} \tag{5.4}$$

Since P and D_{fin} are constant, a variation of PDR also implies a variation of Δ. The PDR is defined in model 1 and therefore, a comparison can be made by plotting the melting time versus PDR.

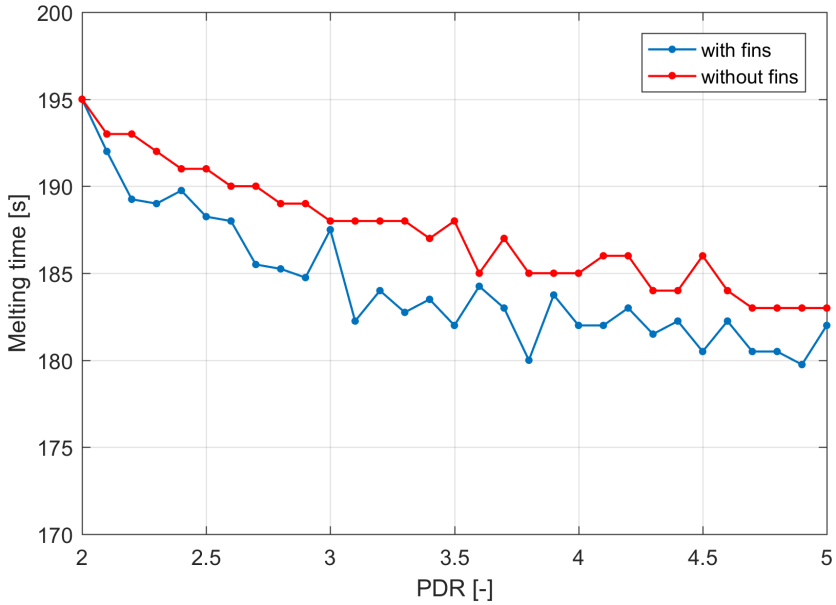

Figure 5.5: Comparison of the results of model 1 and model 3.

In figure 5.5 the following is observed:

1. The blue line and the red line show the same qualitative behaviour.

2. The blue line has a vertical offset with respect to the red line.

This behaviour could be caused by the following variations:

1. The variation of D_{plug} which is equivalent to a variation of the PDR.

2. The variation of the position of the cooling fins with respect to the freeze plug which is represented by Δ.

3. The addition of cooling fins.

In model 1 (red line), it was concluded that the decrease in melting time for a PDR increasing from 2 to 5 is caused by a decrease of D_{plug}. It is likely that in model 3 (blue line) the decrease in melting time is also caused by the decrease of D_{plug}. This explains the similar qualitative behaviour.

Furthermore, it can be concluded that the vertical offset is caused by the addition of cooling fins. The cooling fins result in a better heat transfer from the salt to the alloy. Therefore, more heat is transferred to the freeze plug module and consequently the freeze plug melts faster.

So, the effect of a variation of Δ is not visible for the tested range of PDR values. It can be concluded that the position of the cooling fins with respect to the freeze plugs for the tested range of Δ has no influence on the melting time. However, when Δ is increased beyond the upper limit of 10 mm tested in this model, it can be expected the vertical offset observed in figure 5.5 disappears since heat flowing into the cooling fins at large distances from the edges of the freeze plug will not reach the edges of the freeze plug and therefore, this heat does not contribute to the melting of the freeze plug.

5.2.4. Model 4: Variation of h_{fin}

In this model the influence of h_{fin} is tested. P is fixed at 70 mm, S_L is fixed at 70 mm as, ζ_L=2 and ζ_T=2. D_{fin} is fixed at 35 mm and D_{plug} is fixed at 20 mm. For the model for forced convection across tubes in a tube bank to be valid, $h_{fin} \gg D_{fin}$ must hold. Therefore, h_{fin} ranges from 35 mm to 100 mm. Since the values of ζ_L, ζ_T and D_{fin} are similar to the values taken in model 3, the heat transfer coefficient has not changed. An overview of the parameter values is shown in table 5.4 and the results are displayed in figure 5.6.

Table 5.4: Overview of the parameter values in model 4.

Parameter	Value	Unit
P	70	mm
h_{plug}	40	mm
D_{plug}	20	mm
PDR	3.5	-
S_L	70	mm
h_{fin}	35-100	mm
D_{fin}	35	mm
ζ_L	2	-
ζ_T	2	-
$\langle k \rangle_{fin}$	14275	$\frac{\mathrm{W}}{\mathrm{m^2K}}$
$\langle k \rangle_{top}$	1465	$\frac{\mathrm{W}}{\mathrm{m^2K}}$

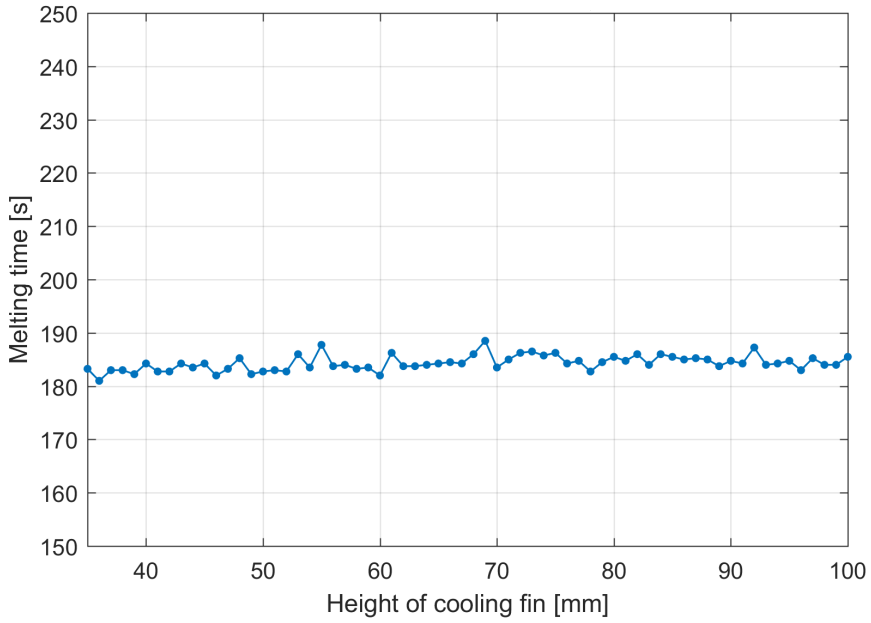

Figure 5.6: Plot of the melting time as a function of the height of the cooling fins.

It can be seen that the variation of h_{fin} has no effect on the melting time. It was expected that for h_{fin} larger than a certain value the effect on the melting time would vanish because heat flowing into the cooling fin near the tip of a large cooling fin will not reach the edge of the freeze plug and therefore, does not contribute to the melting of it. This expectation is not confirmed by the results. However, there is a possibility that when h_{fin} is taken smaller than 35 mm, a change in t_{melt} becomes visible. In model 1, it is derived that for the specified parameter inputs but with h_{fin}=0, the melting time is approximately 200 seconds. It can be expected that for values of h_{fin} lower than 35 mm, t_{melt} approaches 200 seconds.

5.2.5. Model 5: Variation of D_{fin}

In model 5, the effect of the width of the cooling fin on the melting time is investigated. P and S_L are fixed at 70 mm. Δ is fixed at 5 mm. Since the model for the cooling fins is only valid for $1.05 \leq \zeta_L \leq 3$, $1.05 \leq \zeta_T \leq 3$. D_{fin} is computed using the following relation:

$$\frac{S_L}{3} \leq D_{fin} \leq \frac{S_L}{1.3} \tag{5.5}$$

So, D_{fin} is varied from 23.33 mm to 53.5 mm [1]. D_{plug} is determined by using the following relation:

$$D_{plug} = P - D_{fin} - 2\Delta \tag{5.6}$$

Consequently, D_{plug} is varied from 14 mm to 35 mm.

$\langle k \rangle_{fin}$ is dependent on ζ_L, ζ_T and D_{fin}. Since these parameters are varying in this model, $\langle k \rangle_{fin}$ varies as well. An overview of the parameter values is shown in table 5.5 and the results are displayed in figure 5.7.

[1] The values for D_{fin} that result in the $\zeta \leq 1.3$ are omitted because these are not realistic when the assumption of a uniform temperature of the applied flow is made.

Table 5.5: Overview of the parameter values in model 5.

Parameter	Value	Unit
P	70	mm
h_{plug}	40	mm
D_{plug}	6.5-35	mm
PDR	2-10	-
S_L	70	mm
h_{fin}	60	mm
D_{fin}	23.33-53.5	mm
Δ	5	mm
ζ_L	1.3-3	-
ζ_T	1.3-3	-
$\langle k \rangle_{fin}$	13324-14450	$\frac{W}{m^2K}$
$\langle k \rangle_{top}$	1465	$\frac{W}{m^2K}$

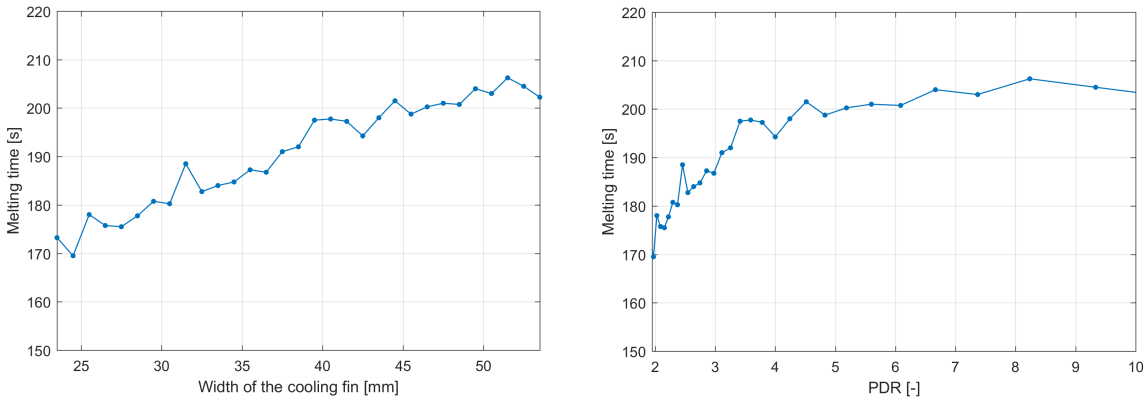

(a) Melting time versus D_{fin}.

(b) Melting time versus the PDR.

Figure 5.7: Plot of the melting time as a function of the width of the cooling fins.

It can be derived that for an increasing width of the cooling fins, the melting time increases. D_{fin} and D_{plug} are related according to equation 5.6. PDR and D_{plug} are related in the following way:

$$PDR = \frac{P}{D_{plug}} \tag{5.7}$$

By combining equation 5.6 and equation 5.7, the following relation is obtained:

$$\frac{P}{PDR} = P - D_{fin} - 2\Delta \tag{5.8}$$

$$PDR = \frac{P}{P - D_{fin} - 2\Delta} \tag{5.9}$$

Since P and Δ are constant, this equation can be used to transform figure 5.7a into figure 5.7b. Note that for increasing D_{fin}, PDR increases as well. By combining figure 5.7b and figure 5.2b, a comparison of model 1 and model 5 can be made. The resulting figure looks as follows.

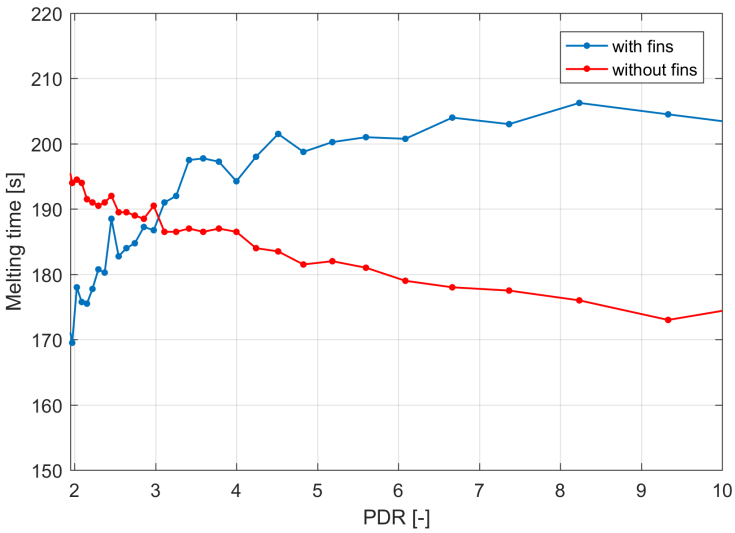

Figure 5.8: Plot of the melting time as a function of the PDR.

The width of the cooling fins seems to have a significant influence on the melting time. An explanation can be found by analysing the temperature distribution within the cooling fins and the freeze plug over time. This temperature distribution is displayed for both a relatively small cooling fin and a relatively large cooling fin in figure 5.9 and 5.10. As was stated in chapter 4, the initial temperature of the freeze plugs and the Hastelloy N including the cooling fins is taken at 773K. The influence of the width of the cooling fins on the melting time can be explained as follows.

1. At t=0, the cooling of the freeze plug module is terminated. The freeze plug, the Hastelloy N around the freeze plugs and the cooling fins have a temperature of 773K.

2. Due to termination of the cooling, heat is transferred from the molten salt to the cooling fins.

3. The temperature of the cooling fins increases and approaches the temperature of the molten salt.

4. The small cooling fin heats up faster than the large cooling fin. The amount of heat flowing into the cooling fins is close to equal. However, the smaller cooling fin has smaller surface that is heated compared to the large fin and therefore, less heat is required to increase the temperature of the fin.

5. The total amount of heat that is conducted from the cooling fin to the alloy around the freeze plug is dependent on the length of the interface between the cooling fin and the alloy around the freeze plug. The length of this interface is equal to D_{fin}. Furthermore, the total amount of heat that is conducted is dependent on the temperature difference across this interface.

6. For a large cooling fin, the stated interface is larger compared to a small cooling fin.

7. The small cooling fin heats up faster than the large cooling fin. For equal times, this results in a larger temperature difference across the stated interface compared to the large cooling fin.

8. Based on the results it can be concluded that the increased temperature difference is dominant in decreasing the melting time in contrast to the increased interface for a large cooling fin.

9. In conclusion, a small cooling fin heats up faster, this results in a larger temperature difference across the interface, a larger total amount of heat is conducted to the edges of the freeze plug and consequently the freeze plug melts faster.

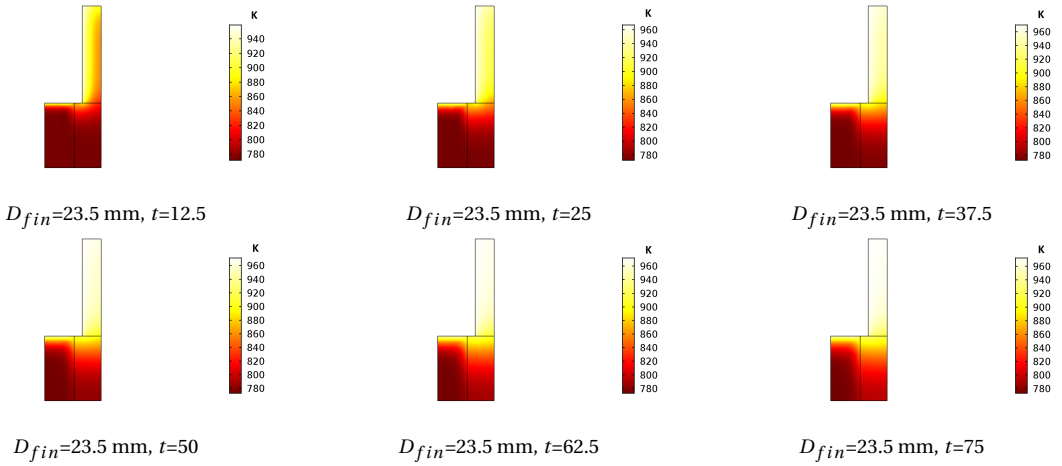

D_{fin}=23.5 mm, t=12.5 D_{fin}=23.5 mm, t=25 D_{fin}=23.5 mm, t=37.5

D_{fin}=23.5 mm, t=50 D_{fin}=23.5 mm, t=62.5 D_{fin}=23.5 mm, t=75

Figure 5.9: Distribution of the temperature in a specific geometry of model 5 for various times, D_{fin}=23.5 mm and the temperature is measured in Kelvin.

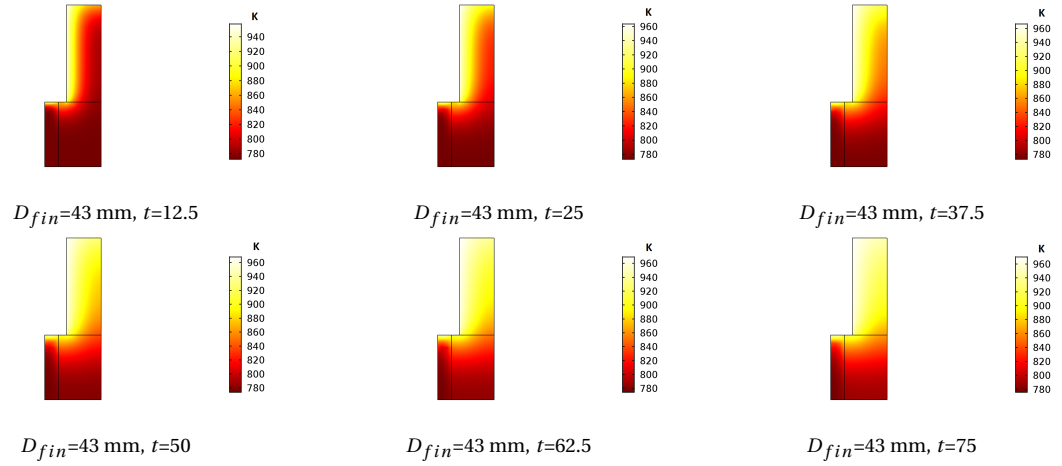

D_{fin}=43 mm, t=12.5 D_{fin}=43 mm, t=25 D_{fin}=43 mm, t=37.5

D_{fin}=43 mm, t=50 D_{fin}=43 mm, t=62.5 D_{fin}=43 mm, t=75

Figure 5.10: Distribution of the temperature in a specific geometry of model 5 for various times, D_{fin}=43 mm and the temperature is measured in Kelvin.

It can thus be concluded that the width of the cooling fin significantly affects the melting time. For the measured conditions the smallest value for D_{fin} proved to be the most efficient. However, in reality it may be impossible to maintain the temperature of the cooling fin at 773K. To obtain a more realistic view, research has to be done on a realistic initial value of the temperature of the cooling fin and the effect of the width of the fin for these values of the initial temperature.

5.3. Results of the 3D models

Below the results of the 3D models are discussed.

5.3.1. Model 6: Variation of PDR by changing P for an in-line arrangement

In model 6, the effect of the spacing of the cooling fins with respect to the freeze plugs on the melting time is investigated. P and S are fixed at 70 mm D_{plug} and D_{fin} are held constant at 30 mm. h_{plug} and h_{fin} are held constant respectively at 40 mm and 100 mm. ζ ranges from 1.4 to 3. Since P=S due to symmetry and D_{fin}=D_{plug}, PDR ranges from 1.4 to 3 as well. The results are displayed in figure 5.11. The behaviour of $\langle k \rangle_{fin}$ is also plotted versus the PDR. This figure is displayed in figure 5.12. An overview of the parameter values is displayed in table 5.6.

Table 5.6: Overview of the parameter values in model 6.

Parameter	Value	Unit
P	42-90	mm
h_{plug}	40	mm
D_{plug}	30	mm
PDR	1.4-3	-
S	42-90	mm
h_{fin}	100	mm
D_{fin}	30	mm
ζ	1.4-3	-
$\langle k \rangle_{fin}$	12356-20597	$\frac{W}{m^2K}$
$\langle k \rangle_{top}$	1465	$\frac{W}{m^2K}$

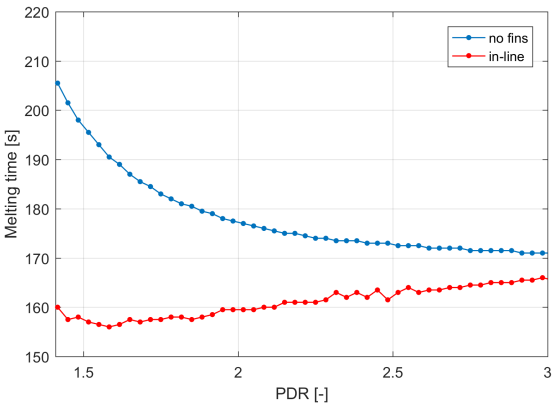

Figure 5.11: Plot of the PDR versus the melting time for model 6.

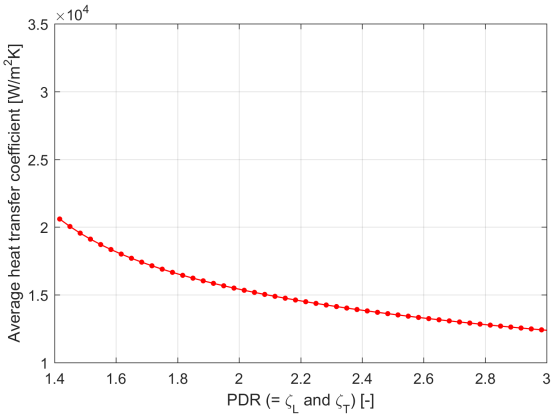

Figure 5.12: Behaviour of $\langle k \rangle_{fin}$ for PDR in model 6.

The blue line represents the geometry without cooling fins. The melting time as a function of the PDR behaves similarly as was observed in 2D in figure 5.3b. A possible explanation for this behaviour is that for small values of the PDR, the amount of Hastelloy N between adjacent freeze plug will be limited. This results in a reduction of the amount of heat that can flow into the alloy and therefore, the plug melts slower at the edges. However, when the amount of metal between the plugs reaches a certain width, the influence levels off. By using cooling fins, a significant reduction in the melting time is observed for small values of the PDR. By using cooling fins, an increase of the surface where heat transfer by convection takes place is achieved and consequently more heat is transferred to the freeze plug system. This results in a decrease of the melting time compared to a freeze plug system without cooling fins.

In figure 5.11 it can be observed that for decreasing PDR, the melting time decreases. In figure 5.12 it can be observed that for low values of the PDR, the heat transfer coefficient is larger. Therefore, for low values of the PDR more heat is transferred to the cooling fins and consequently t_{melt} decreases.

5.3.2. Model 7: Variation of ζ by changing S for a staggered arrangement

In model 7, the effect of the spacing of the cooling fins with respect to the freeze plugs on the melting time is investigated for a staggered arrangement. D_{plug} and D_{fin} are held constant at 30 mm. h_{plug} and h_{fin} are held constant respectively at 40 mm and 100 mm. ζ ranges from 2 to 3. The reason for letting ζ start at 2 is because for ζ smaller than 2, the freeze plug and the cooling fins overlap. The results are displayed in figure 5.13. The behaviour of $\langle k \rangle_{fin}$ is also plotted versus ζ. This figure is displayed in figure 5.14. An overview of the parameter values is displayed in table 5.7.

Table 5.7: Overview of the parameter values in model 7.

Parameter	Value	Unit
ζ	2-3	-
h_{plug}	40	mm
D_{plug}	30	mm
S	60-90	mm
h_{fin}	100	mm
D_{fin}	30	mm
$\langle k \rangle_{fin}$	12554-16325	$\frac{W}{m^2K}$
$\langle k \rangle_{top}$	1465	$\frac{W}{m^2K}$

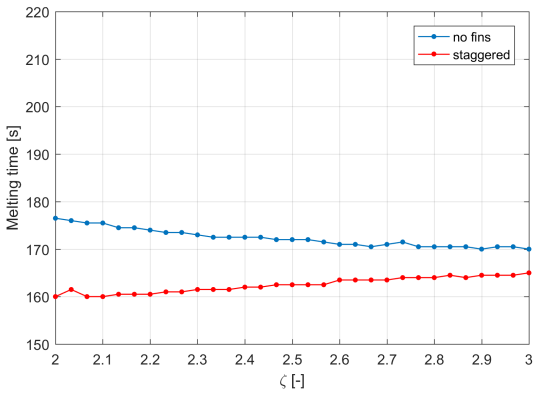

Figure 5.13: Plot of the ζ versus the melting time for model 7.

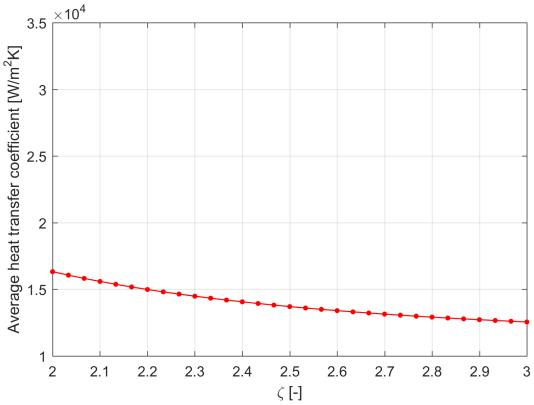

Figure 5.14: Behaviour of $\langle k \rangle_{fin}$ for ζ in model 7.

In figure 5.13 it can be seen that the results are almost similar to figure 5.11 for PDR larger than 2. This can explained by comparing figure 5.12 and figure 5.14, it can be derived that the average heat transfer coefficient is slightly bigger for the staggered arrangement in comparison to the in-line arrangement. This was already predicted by the model in chapter 2 for relative widely spaced tube arrangements. Because the amount of heat that is transferred to the cooling fins is almost similar for both arrangements, it is expected that the melting times for the freeze plugs in both arrangements are similar as well.

5.3.3. Model 8: Variation of ζ by changing D_{fin} for an in-line arrangement

In model 8, the effect of the diameter of the cooling fins on the melting time is investigated for an in-line arrangement. In model 5 it was observed that the diameter of the cooling fins has a significant effect on the melting time. The effect was caused by the initial temperature of the cooling fins. The initial temperature of the plug system including the cooling fins was equal to 773K in all previous tested models. In reality, it may be impossible to maintain the temperature of the cooling fins at this temperature. The surface of the cooling fins is in contact with the molten salt of 973K. It can be expected that the initial temperature of the cooling fins has a value somewhere between 773K and 973K. Therefore, model 8 is performed two times. One time for T_0=773K and one time for T_0=973K. S and P are both equal to 70 mm, D_{plug} is equal to 30 mm, D_{fin} ranges from 23.33 mm to 50 mm. The melting time for the geometry without cooling fins is taken from figure 5.11 and is plotted for comparison. The results are displayed in figure 5.15 and 5.16. An overview of the parameter values is displayed in table 5.8.

Table 5.8: Overview of the parameter values in model 8.

Parameter	Value	Unit
P	70	mm
h_{plug}	40	mm
D_{plug}	30	mm
PDR	1.4-3	-
S	70	mm
h_{fin}	100	mm
D_{fin}	23.33-50	mm
ζ	1.4-3	-
$\langle k \rangle_{fin}$	14047-16188	$\frac{W}{m^2K}$
$\langle k \rangle_{top}$	1465	$\frac{W}{m^2K}$

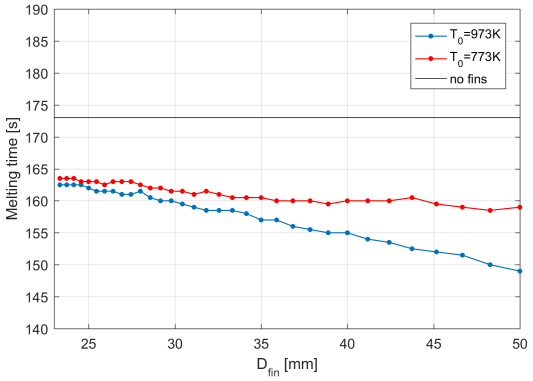

Figure 5.15: Plot of D_{fin} versus the melting time for model 8.

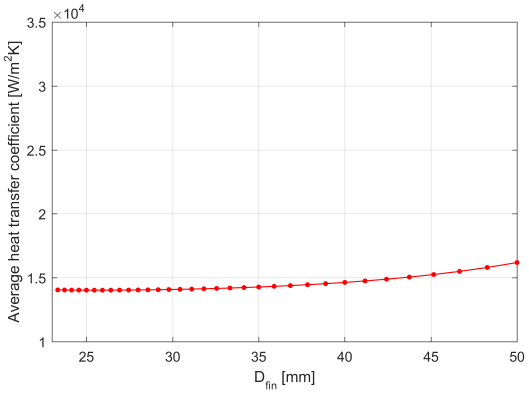

Figure 5.16: Behaviour of $\langle k \rangle_{fin}$ for D_{fin} in model 8.

In figure 5.15, it can be derived that an increase in D_{fin} results in a decrease of t_{melt} for both values of T_0. In 2D the effect was adversely. This can be explained by the fact that heating of a 3D cylindrical cooling fin is more efficient than heating the rectangular shape in 2D. In 3D the fin is heated radially inwards. The surface of a rectangular in 2D where convective heat transfer occurs is relatively small compared to the area that is heated. A cylinder in 3D has a larger surface compared to the volume of the cylinder. Therefore, relatively more heat is transferred to the cylinder in contrast to a 2D rectangular and consequently the temperature of a cylinder increases faster.

Furthermore, it can be observed that the difference between the red line and blue line in figure 5.15 increases for increasing values of D_{fin}. An explanation for this is the following.

1. Consider the cooling fins with T_0=773K. At t=0, heat penetrates into the cooling fins and consequently the temperature of the cooling fins is increased.

2. A larger D_{fin} means a larger volume of alloy that has to be heated and consequently a larger amount of heat is required.

3. To transfer a larger amount of heat from the molten salt to the cooling fins, a larger amount of time is needed. So, the time it takes to increase the cooling fins from 773K to 973K increases for increasing D_{fin}.

4. For this reason, the heat conducted to the freeze plug by cooling fins with T_0=973K is larger for a longer amount of time compared to the the heat conducted to the freeze plug by cooling fins with T_0=773K.

5. It can be expected that the difference between the red line and blue line in figure 5.15 increases for increasing values of D_{fin}.

6

Conclusions & Recommendations

6.1. Conclusions

The goal of this thesis is to discover how cooling fins can be integrated in the design of the freeze plug in order to achieve a decrease in the time it takes to melt the freeze plug. First of all, research is done on the effects of the arrangement and the geometrical parameters of tube banks on the heat transfer in tube banks. It was found that the heat transfer depends on the average heat transfer coefficient, the total surface area of the tube bank and the average temperature gradient. For the conditions obliged by the reactor, the following conclusions can be drawn.

- The heat transfer coefficient of a cylinder in a tube bank is positively influenced by a decreasing longitudinal pitch for both a staggered arrangement and a in-line arrangement.
- Increase of the Reynolds number leads to a significant increase in the average heat transfer coefficient of a tube bank and is the dominant parameter for enhancing the heat transfer.
- Increasing the transversal pitch is beneficial for staggered arrangements. However, there should be noted that decreasing of the transverse pitch leads to an increase in the Reynolds number when a constant applied flow is assumed. Since the Reynolds number is the dominant parameter it is likely that this effect will dominate the influence of the transversal pitch.
- Particularly for closely spaced tube banks, staggered arrangements perform better than in-line arrangements.

The influence of the diameter of the freeze plug and the width of the Hastelloy N on the melting time for a geometry without cooling fins were examined. It was found that the width of the Hastelloy N between the freeze plugs has a major influence on the melting time. For a width smaller than 40 mm the melting time increases exponentially. For a width larger than 40 mm, the melting time remains close to constant. Therefore, to obtain an efficient melting process the width of the Hastelloy N must be taken larger than 40 mm. The diameter of the freeze plug only had a minor influence on the melting time.

When cooling fins were added to the geometry, it was shown that the melting time could be decreased significantly. The exponential increase of the melting time for values of the width of the Hastelloy N between the freeze plugs smaller than 40 mm was not observed anymore. Instead, a linear decrease in melting time was observed for decreasing values of this width. It can be concluded that using cooling fins for closely packed arrangements of freeze plugs is highly useful. For the closest packed arrangements that were tested, a decrease in melting time of 25% could be achieved by using cooling fins.

What concerns the height of the cooling fins, no variation in melting time was observed for various values of the height. However, the height must be chosen sufficiently large in order to justify the use of the theory on tube banks.

At last, it was shown that the melting time of the freeze plugs depends on the initial temperature of the cooling fins and the diameter of the cooling fins. In reality the value of the initial value of the cooling fins is somewhere between the temperature of the freeze plug module and the temperature of the molten salt. These temperatures are considered to be respectively the minimum and the maximum value of the initial

temperature in reality. For 3D models, it was shown that the melting time decreases for increasing diameter of the cooling fins. This effect was strengthened when the initial temperature of the cooling fins was increased from the minimum value to the maximum value. It can be concluded that the influence of the diameter of the cooling fins on the melting time is strongly dependent on the initial temperature of the cooling fins.

On the whole, in 3D, the most optimal configuration of a tube bank in combination with an arrangement of freeze plugs, consists of a closely spaced arrangement of cylinders with a large diameter.

6.2. Recommendations

In this thesis assumptions had to be made. To gain a better understanding of the agreement of the results with reality, these assumptions should be tested. Besides, there is still opportunity for further optimisation of design including coolings fins. Therefore, the following recommendations are made.

- *Finding the minimum h_{plug} to prevent the plug from collapsing.*
  The melting time is strongly dependent on the height of the plug. The smaller the height of the freeze plug, the smaller the melting time. Therefore, it is valuable for the melting time to minimize this property as much as possible.

- *Adding the drainage time to the tested geometries.*
  The speed of the drainage of the reactor core is a combination of the speed of the melting process and the drainage process. The drainage time for the tested configurations has not been taken into account. For an efficient draining process, the freeze plugs must be placed as close to each other as possible. However, this conflicts with the requirements for an efficient melting process. Therefore, further research has to be done on the influence of cooling fins on the drainage time.

- *Finding the properties of the solid salt.*
  A substitute salt has been used for the calculations and computations. However, it is unknown whether this is a valid substitution. The actual properties of the solid salt have to be determined. It will either prove that LiCl is a valid substitution or it makes further research possible with a higher accuracy.

- *Using an additional layer of a material with a higher thermal conductivity.*
  In a previous research [14] an additional layer of material was used to fill the intermediate space between the freeze plugs. This material had a higher thermal conductivity than Hastelloy N. This design may prove to be even more valuable for a design with cooling fins since it reduces it enhances the heat transfer from the cooling fin into the freeze plug module.

- *Research on a realistic initial temperature of the cooling fins.*
  This research showed that the initial temperature of the cooling fins have a significant result on the melting time, particularly for cooling fins with a large radius. A better understanding of the temperature the cooling fins can be maintained on results in more accurate results.

- *Research on the development of the temperature gradient as a function of position and time for various tube banks.*
  When a fluid flows through a tube bank, heat is transferred and consequently the temperature decreases. Therefore, at downstream cylinder rows the temperature gradient will be smaller. By taking an average of the temperature gradient in the tube bank, more accurate results can be obtained. The temperature also variates over time due to the heating of the core in case of a black-out. This compensates to some extent for the temperature decrease in the tube bank. However, the ratio between these two is unknown.

- *Further optimisation of tube bank parameters.*
  In this thesis not all possible 3D configurations and only cylindrical cooling fins are tested. By changing the shape of the cooling fins an even better heat transfer may be obtained. By testing other combinations of a freeze plug grid and a cooling fin grid, faster combinations may be discovered.

Bibliography

[1] M. Brovchenko, D. Heuer, E. Merle-Lucotte, M. Allibert, V. Ghetta, A. Laureau, and P. Rubiolo. Design-related studies for the preliminary safety assessment of the molten salt fast reactor. *Nuclear Science and Engineering*, 175:329–339, November 2013.

[2] D.Sumner. *Circular Cylinders in Cross-flow*. PhD thesis, McGill University, 1999.

[3] Generation IV International Forum. Molten salt reactors (msr). URL `https://www.gen-4.org/gif/jcms/c_9359/msr`. Online; accessed 2 May 2017.

[4] L. Frima. Burnup in a molten salt fast reactor. Master's thesis, Delft University of Technology, September 2013.

[5] V. Ignatiev, O. Feynberg, A. Merzlyakov, A. Surenkov, A. Zagnitko, V. Afonichkin, A. Bovet, V. Khokhlov, V. Subbotin, R. Fazilov, M. Gordeev, A. Panov, and A. Toropov. Progress in development of MOSART concept with Th support. January 2012.

[6] F.P. Incropera, D.P. DeWitt, T. Bergmann, and A. Lavine. *Fundamentals of Heat and Mass Transfer*. John Wiley and Sons, sixth edition, 2002.

[7] W.A. Khan, J.R. Culham, and M.M. Yovanovich. Convection heat transfer from tube banks in crossflow: Analytical approach. *International Journal of Heat and Mass Transfer*, 49(25–26):4831 – 4838, 2006.

[8] J.L. Kloosterman. Lessen uit japan, January 2012. URL `http://www.janleenkloosterman.nl/ntvn_201201.php`. Online; accessed 4 May 2017.

[9] A. Makkinje. Design of a freeze plug grate. Bachelor's thesis, Delft University of Technology, February 2016.

[10] H. E. McCoy, W. H. Cook, R.E. Gehlback, J.R. Weir Jr., C.R. Kennedy, C.E. Sessions, R.L. Beatty, A.P. Litman, and J.W.Koger. Materials for molten-salt reactors. *Journal of Nuclear Applications*, May 1969.

[11] J. Serp, M. Allibert, O. Beneš, S. Delpech, O. Feynberg, V. Ghetta, D. Heuer, D. Holcomb, V. Ignatiev, J.L. Kloosterman, L. Luzzi, E. Merle-Lucotte, J. Uhlíř, R. Yoshioka, and D. Zhimin. The molten salt reactor (MSR) in generation iv: Overview and perspectives. *Progress in Nuclear Energy*, 77:308 – 319, 2014.

[12] P. Swaroop. Design of a freeze plug for the molten salt reactor (msr). Master's thesis, Delft University of Technology, September 2015.

[13] H. van den Akker and R. Mudde. *Fysische Transportverschijnselen*. Delft Academic Press, fourth edition, 2014.

[14] F. van Tuyll. A new design for the safety plug in a molten salt fast reactor. Bachelor's thesis, Delft University of Technology, December 2016.

[15] A. Žukauskas. Heat transfer from tubes in crossflow. *Advances in Heat Transfer*, 8:93 – 160, 1972.

A

Matlab Scripts

A.1. Calculating t_{melt}

The following script is used to calculate t_{melt} using tables generated by COMSOL. The script shown is used for model 3. However, similar scripts were used for the remaining models.

```
%% Berekening t_melt model 3
clear all;
close all;
clc;

%% Data+Variabelen
COMSOL = readtable('P=70,PDR=(2,0.1,5),Rfin=17.5,zetaL=2,zetaT=2,tstep=0.25,Model3.csv');
Data=COMSOL(:,2:end);
Data= table2array(Data);
%COMSOL ran for varying r_FP
P=70;                           %Distance between two adjacent freeze plugs
%r_FP =7:0.5:17.5;              %Radius Freeze Plug
%PDR=P./(2.*r_FP);              %PDR ratio

%COMSOL ran for varying PDR
PDR=2:0.1:5;                    %PDR ratio
r_FP =(P./PDR).*0.5;
ts = 0.25;                      %Time step used in your data
Dfin=35;
delta=0.5.*(P-2.*r_FP-Dfin);

%% Berekening tmelt voor verschillende R_plug
[sel,z] = min( Data~=0, [], 1 );
z = z*ts;                       %time needed to fully melt the freeze plug in seconds
tmz = zeros(size(Data,2)/length(r_FP),length(r_FP));
for i = 1:size(Data,2)/length(r_FP)
    tmz(i,1:length(r_FP))=z(1+length(r_FP)*(i-1):length(r_FP)*i);
end

%% Export CSV Table
Final_Solution=[r_FP' delta' PDR' tmz'];
headers = {'Radius_plug','delta' 'P_over_D_Ratio', 'Melting_time',};
table=array2table(Final_Solution,'VariableNames',headers);
writetable(table,'Model3_tabel.csv')

%% Plotting P vs Tmelt
width = 6;      %Width in inches
height = 4;     %Height in inches
alw = 0.75;     %Axes Line Width
```

```
fsz = 10;        %Fontsize
lw = 0.8;        %Line Width
msz = 12;         %Marker Size

pos =get(gcf,'Position');
set(gcf,'Position', [pos(1) pos(2) width*100, height*100]);   %<-Setsize
set(gca,'FontSize',fsz,'LineWidth', alw) ;%<?-Setproperties
plot(delta,tmz,'.-','LineWidth',lw ,'MarkerSize',msz) ;%<-Specifyplotproperites
axis([0 10.5 170 205]);
xlabel('Distance between edge of the plug and edge of the cooling fin [mm]') ;
ylabel( 'Melting time [s]');
title('Melting time for various values of delta');
grid on

set(gcf,'InvertHardcopy', 'on');
set(gcf,'PaperUnits' , 'inches' );
papersize =get(gcf, 'PaperSize' );
left = (papersize(1)-width)/2;
bottom = (papersize(2)-height )/2;
myfiguresize = [ left , bottom , width , height ];
set(gcf,'PaperPosition', myfiguresize ) ;

%Save the file as PNG
print('Tmelt_vs_delta_Model3', '-dpng' , '-r300 ') ;

figure
%% Plotting PDR vs Tmelt

pos =get(gcf,'Position' );
set(gcf,'Position' , [pos(1) pos(2) width*100, height*100]);   %<-Setsize
set(gca,'FontSize',fsz,'LineWidth', alw) ;%<?-Setproperties
plot(PDR,tmz,'.-','LineWidth',lw ,'MarkerSize',msz) ;%<-Specifyplotproperites
axis([2 5 170 205]);
xlabel('PDR [-]') ;
ylabel( 'Melting time [s]');
title('Melting time for various values of delta');
grid on

set(gcf,'InvertHardcopy', 'on');
set(gcf,'PaperUnits' , 'inches' );
papersize =get(gcf, 'PaperSize' );
left = (papersize(1)-width)/2;
bottom = (papersize(2)-height )/2;
myfiguresize = [ left , bottom , width , height ];
set(gcf,'PaperPosition', myfiguresize ) ;

%Save the file as PNG
print('Tmelt_vs_PDR_Model3', '-dpng' , '-r300 ') ;
```

A.2. Calculating $\langle k \rangle_{top}$

```
%%computing average Nusselt number for forced convection across a flat plate.
clear all
close all
clc

T=973;
Rpipe=0.06;
rho=(4.094-8.82*10^-4*(T-1008))*10^3;
v=2;
```

```
nu=5.54*10^-8*exp(3689/T);
L=2*Rpipe;
mu=rho*5.54*10^-8*exp(3689/T);
Cp=(-1.111+0.00278*T)*10^3;
lambda=0.928+8.397*10^-5*T;

Re=(rho*v*L)/mu;
Pr=(Cp*mu)/lambda;

Nu=0.221*((Re)^(1/2))*((Pr)^(1/3));
h=Nu*(lambda/L);
```

A.3. Calculating $\langle k \rangle_{fin}$

```

%% Computing average Nusselt number for forced convection across a cooling fin for a varying
    SL due to a varying Dfin.
clc
close all
clear all

T=973;
rho=(4.094-8.82*10^-4*(T-1008))*10^3;
vapplied=2;
nu=5.54*10^-8*exp(3689/T);
mu=rho*5.54*10^-8*exp(3689/T);
Cp=(-1.111+0.00278*T)*10^3;
lambda=0.928+8.397*10^-5*T;
delta=0.005;

SL=0.07;                                                %Longitudinal distance between
    two consecutive tubes.                                                  %and the
    simulation will take too long.
P=0.07;
Dfin=0.0235:0.0005:0.0535;
ZL=SL./Dfin;
ZT=2;

Dplug=P-Dfin-(2.*delta);
PDR=SL./Dplug;

C=(0.25+exp(-0.55.*ZL)).*ZT.^(0.285).*ZL.^(0.212);      %correction coefficient in-line array

v=(ZT/(ZT-1))*vapplied;

Re=(rho.*v.*Dfin)./mu;
Pr=(Cp.*mu)./lambda;
Nu=C.*((Re).^(1/2)).*((Pr).^(1/3));

h=Nu.*(lambda./Dfin);

%% Constructing a table
finalvalues=[PDR' ZL' Nu' Dfin' h'];
headers = {'P_over_D_Ratio','ZetaL','Average_Nusselt_Number','Diameter_fin','
    Heat_Transfer_Coefficient'};
tablevalues=array2table(finalvalues,'VariableNames',headers);
writetable(tablevalues,'Dfin=(23.5,0.5,53.5)_Nusselt_values,Model5.csv')

cellarray1={'h_conv'};
for i=1:length(h)
cellarray1{1,1+i}=h(i);
```

```
end
cell2csv('{COMSOL}_Dfin=(23.5,0.5,53.5)_h_conv,Model5.csv',cellarray1,',',1997,'.')

cellarray2={'D_fin'};
for i=1:length(Dfin)
cellarray2{1,1+i}=Dfin(i);
end
cell2csv('{COMSOL}_Dfin=(23.5,0.5,53.5)_D_fin_values,Model5.csv',cellarray2,',',1997,'.')
```

A.4. Exporting variables to COMSOL

The following script is used to configure the results of a variable to make them importable in COMSOL.

```
function cell2csv(fileName, cellArray, separator, excelYear, decimal)
% Writes cell array content into a *.csv file.
%
% CELL2CSV(fileName, cellArray, separator, excelYear, decimal)
%
% fileName     = Name of the file to save. [ i.e. 'text.csv' ]
% cellArray    = Name of the Cell Array where the data is in
% separator    = sign separating the values (default = ';')
% excelYear    = depending on the Excel version, the cells are put into
%                quotes before they are written to the file. The separator
%                is set to semicolon (;)
% decimal      = defines the decimal separator (default = '.')


%% Checking for optional variables
if ~exist('separator', 'var')
    separator = ',';
end

if ~exist('excelYear', 'var')
    excelYear = 1997;
end

if ~exist('decimal', 'var')
    decimal = '.';
end

%% Setting separator for newer excelYears
if excelYear > 2000
    separator = ';';
end

%% Write file
datei = fopen(fileName, 'w');

for z=1:size(cellArray, 1)
    for s=1:size(cellArray, 2)

        var = eval(['cellArray{z,s}']);
        % If zero, then empty cell
        if size(var, 1) == 0
            var = '';
        end
        % If numeric -> String
        if isnumeric(var)
            var = num2str(var);
            if decimal ~= '.'
                var = strrep(var, '.', decimal);
            end
```

```
50          end
51          % If logical -> 'true' or 'false'
52          if islogical(var)
53              if var == 1
54                  var = 'TRUE';
55              else
56                  var = 'FALSE';
57              end
58          end
59          % If newer version of Excel -> Quotes 4 Strings
60          if excelYear > 2000
61              var = ['"' var '"'];
62          end
63
64          % OUTPUT value
65          fprintf(datei, '%s', var);
66
67          % OUTPUT separator
68          if s ~= size(cellArray, 2)
69              fprintf(datei, separator);
70          end
71      end
72      if z ~= size(cellArray, 1) % prevent a empty line at EOF
73          % OUTPUT newline
74          fprintf(datei, '\n');
75      end
76  end
77  % Closing file
78  fclose(datei);
79  end
```

B

Tables

B.1. Results model 1

Table B.1: Values of the parameters in model 1.

R_plug [mm]	PDR	tmelt [s]
7	5	183
9	3.9	185
11	3.2	189
13	2.7	193
15	2.3	194
17	2.1	195
19	1.8	199
21	1.7	204
23	1.5	210
25	1.4	220
27	1.3	239
29	1.2	275
31	1.1	349
33	1.1	619

B.2. Results model 2

Table B.2: Values of the parameters in model 2.

P [mm]	PDR	tmelt [s]
36	1.2	422
38	1.3	342
40	1.3	290
42	1.4	272
44	1.5	249
46	1.5	239
48	1.6	228
50	1.7	219
52	1.7	213
54	1.8	211
56	1.9	205
58	1.9	202
60	2	200

P [mm]	PDR	tmelt [s]
62	2.1	197
64	2.1	197
66	2.2	194
68	2.3	193
70	2.3	191
72	2.4	190
74	2.5	191
76	2.5	188
78	2.6	190
80	2.7	188
82	2.7	187
84	2.8	186
86	2.9	188
88	2.9	189
90	3	185
92	3.1	186
94	3.1	186
96	3.2	185
98	3.3	184
100	3.3	185
102	3.4	189
104	3.5	185
106	3.5	185
108	3.6	184
110	3.7	184
112	3.7	185
114	3.8	188
116	3.9	184
118	3.9	184
120	4	188
122	4.1	188
124	4.1	185
126	4.2	184
128	4.3	186
130	4.3	184
132	4.4	184
134	4.5	185
136	4.5	183
138	4.6	184
140	4.7	185
142	4.7	185
144	4.8	187
146	4.9	187
148	4.9	185
150	5	187

B.3. Results model 3

Table B.3: Values of the parameters in model 3.

Rplug [mm]	Delta [mm]	PDR	tmelt [s]	delta_t_model1 [s]
17.5	0	2	195	0
16.7	0.8	2.1	192	-1
15.9	1.6	2.2	189	-4
15.2	2.3	2.3	189	-3

Rplug [mm]	Delta [mm]	PDR	tmelt [s]	delta_t_model1 [s]
14.6	2.9	2.4	190	-1
14	3.5	2.5	188	-3
13.5	4	2.6	188	-2
13	4.5	2.7	186	-5
12.5	5	2.8	185	-4
12.1	5.4	2.9	185	-4
11.7	5.8	3	188	-1
11.3	6.2	3.1	182	-6
10.9	6.6	3.2	184	-4
10.6	6.9	3.3	183	-5
10.3	7.2	3.4	184	-4
10	7.5	3.5	182	-6
9.7	7.8	3.6	184	-1
9.5	8	3.7	183	-4
9.2	8.3	3.8	180	-5
9	8.5	3.9	184	-1
8.8	8.8	4	182	-3
8.5	9	4.1	182	-4
8.3	9.2	4.2	183	-3
8.1	9.4	4.3	182	-3
8	9.5	4.4	182	-2
7.8	9.7	4.5	181	-6
7.6	9.9	4.6	182	-2
7.4	10.1	4.7	181	-3
7.3	10.2	4.8	181	-3
7.1	10.4	4.9	180	-3
7	10.5	5	182	-1

B.4. Results model 4

Table B.4: Values of the parameters in model 4.

hfin [mm]	tmelt [s]
35	183
36	181
37	183
38	183
39	182
40	184
41	183
42	183
43	184
44	184
45	184
46	182
47	183
48	185
49	182
50	183
51	183
52	183
53	186
54	184
55	188
56	184

hfin [mm]	tmelt [s]
57	184
58	183
59	184
60	182
61	186
62	184
63	184
64	184
65	184
66	185
67	184
68	186
69	189
70	184
71	185
72	186
73	187
74	186
75	186
76	184
77	185
78	183
79	185
80	186
81	185
82	186
83	184
84	186
85	186
86	185
87	185
88	185
89	184
90	185
91	184
92	187
93	184
94	184
95	185
96	183
97	185
98	184
99	184
100	186

B.5. Results model 5

Table B.5: Values of the parameters in model 5.

Dfin [mm]	Rplug [mm]	PDR	tmelt [s]	k_conv [W/m^2K]	delta_t_model1 [s]
23.5	18.25	1.9	173	14450	-24
24.5	17.75	2	170	14452	-25
25.5	17.25	2	178	14452	-17
26.5	16.75	2.1	176	14448	-18
27.5	16.25	2.2	176	14441	-16

Dfin [mm]	Rplug [mm]	PDR	tmelt [s]	k_conv [W/m^2K]	delta_t_model1 [s]
28.5	15.75	2.2	178	14430	-13
29.5	15.25	2.3	181	14416	-10
30.5	14.75	2.4	180	14398	-11
31.5	14.25	2.5	189	14377	-4
32.5	13.75	2.5	183	14352	-7
33.5	13.25	2.6	184	14323	-6
34.5	12.75	2.7	185	14292	-4
35.5	12.25	2.9	187	14258	-1
36.5	11.75	3	187	14221	-4
37.5	11.25	3.1	191	14182	5
38.5	10.75	3.3	192	14140	6
39.5	10.25	3.4	198	14096	11
40.5	9.75	3.6	198	14050	11
41.5	9.25	3.8	197	14003	10
42.5	8.75	4	194	13953	8
43.5	8.25	4.2	198	13903	14
44.5	7.75	4.5	202	13851	18
45.5	7.25	4.8	199	13797	17
46.5	6.75	5.2	200	13743	18
47.5	6.25	5.6	201	13688	20
48.5	5.75	6.1	201	13632	22
49.5	5.25	6.7	204	13575	26
50.5	4.75	7.4	203	13518	26
51.5	4.25	8.2	206	13460	30
52.5	3.75	9.3	205	13401	32
53.5	3.25	10.8	202	13342	26

B.6. Results model 6

Table B.6: Values of the parameters in model 6.

S [mm]	zeta	tmelt [s]	k_conv [W/m^2K]	P [mm]	PDR	tmelt_nofins [s]	delta_t_melt [s]
42.5	1.42	160	20597	42.5	1.42	205.5	-45.5
43.5	1.45	157.5	20046	43.5	1.45	201.5	-44
44.5	1.48	158	19554	44.5	1.48	198	-40
45.5	1.52	157	19112	45.5	1.52	195.5	-38.5
46.5	1.55	156.5	18712	46.5	1.55	193	-36.5
47.5	1.58	156	18346	47.5	1.58	190.5	-34.5
48.5	1.62	156.5	18011	48.5	1.62	189	-32.5
49.5	1.65	157.5	17701	49.5	1.65	187	-29.5
50.5	1.68	157	17414	50.5	1.68	185.5	-28.5
51.5	1.72	157.5	17147	51.5	1.72	184.5	-27
52.5	1.75	157.5	16897	52.5	1.75	183	-25.5
53.5	1.78	158	16663	53.5	1.78	182	-24
54.5	1.82	158	16442	54.5	1.82	181	-23
55.5	1.85	157.5	16234	55.5	1.85	180.5	-23
56.5	1.88	158	16037	56.5	1.88	179.5	-21.5
57.5	1.92	158.5	15849	57.5	1.92	179	-20.5
58.5	1.95	159.5	15671	58.5	1.95	178	-18.5
59.5	1.98	159.5	15501	59.5	1.98	177.5	-18
60.5	2.02	159.5	15339	60.5	2.02	177	-17.5
61.5	2.05	159.5	15184	61.5	2.05	176.5	-17
62.5	2.08	160	15035	62.5	2.08	176	-16
63.5	2.12	160	14892	63.5	2.12	175.5	-15.5
64.5	2.15	161	14755	64.5	2.15	175	-14

S [mm]	zeta	tmelt [s]	k_conv [W/m^2K]	P [mm]	PDR	tmelt_nofins [s]	delta_t_melt [s]
65.5	2.18	161	14622	65.5	2.18	175	-14
66.5	2.22	161	14495	66.5	2.22	174.5	-13.5
67.5	2.25	161	14372	67.5	2.25	174	-13
68.5	2.28	161.5	14253	68.5	2.28	174	-12.5
69.5	2.32	163	14138	69.5	2.32	173.5	-10.5
70.5	2.35	162	14027	70.5	2.35	173.5	-11.5
71.5	2.38	163	13919	71.5	2.38	173.5	-10.5
72.5	2.42	162	13815	72.5	2.42	173	-11
73.5	2.45	163.5	13714	73.5	2.45	173	-9.5
74.5	2.48	161.5	13615	74.5	2.48	173	-11.5
75.5	2.52	163	13520	75.5	2.52	172.5	-9.5
76.5	2.55	164	13427	76.5	2.55	172.5	-8.5
77.5	2.58	163	13337	77.5	2.58	172.5	-9.5
78.5	2.62	163.5	13249	78.5	2.62	172	-8.5
79.5	2.65	163.5	13164	79.5	2.65	172	-8.5
80.5	2.68	164	13081	80.5	2.68	172	-8
81.5	2.72	164	13000	81.5	2.72	172	-8
82.5	2.75	164.5	12921	82.5	2.75	171.5	-7
83.5	2.78	164.5	12844	83.5	2.78	171.5	-7
84.5	2.82	165	12769	84.5	2.82	171.5	-6.5
85.5	2.85	165	12696	85.5	2.85	171.5	-6.5
86.5	2.88	165	12625	86.5	2.88	171.5	-6.5
87.5	2.92	165.5	12555	87.5	2.92	171	-5.5
88.5	2.95	165.5	12487	88.5	2.95	171	-5.5
89.5	2.98	166	12421	89.5	2.98	171	-5
90.5	3.02	165.5	12356	90.5	3.02	171	-5.5

B.7. Results model 7

Table B.7: Values of the parameters in model 7.

S [mm]	zeta	tmelt [s]	k_conv [W/m^2K]	P [mm]	PDR	tmelt_nofins [s]	delta_tmelt [s]
60	2	160	16325	60	2	176.5	-16.5
61	2.03	161.5	16064	61	2.03	176	-14.5
62	2.07	160	15820	62	2.07	175.5	-15.5
63	2.1	160	15592	63	2.1	175.5	-15.5
64	2.13	160.5	15378	64	2.13	174.5	-14
65	2.17	160.5	15177	65	2.17	174.5	-14
66	2.2	160.5	14989	66	2.2	174	-13.5
67	2.23	161	14811	67	2.23	173.5	-12.5
68	2.27	161	14644	68	2.27	173.5	-12.5
69	2.3	161.5	14486	69	2.3	173	-11.5
70	2.33	161.5	14338	70	2.33	172.5	-11
71	2.37	161.5	14197	71	2.37	172.5	-11
72	2.4	162	14065	72	2.4	172.5	-10.5
73	2.43	162	13939	73	2.43	172.5	-10.5
74	2.47	162.5	13820	74	2.47	172	-9.5
75	2.5	162.5	13707	75	2.5	172	-9.5
76	2.53	162.5	13600	76	2.53	172	-9.5
77	2.57	162.5	13499	77	2.57	171.5	-9
78	2.6	163.5	13403	78	2.6	171	-7.5
79	2.63	163.5	13311	79	2.63	171	-7.5
80	2.67	163.5	13224	80	2.67	170.5	-7
81	2.7	163.5	13142	81	2.7	171	-7.5
82	2.73	164	13063	82	2.73	171.5	-7.5

S [mm]	zeta	tmelt [s]	k_conv [W/m^2K]	P [mm]	PDR	tmelt_nofins [s]	delta_tmelt [s]
83	2.77	164	12988	83	2.77	170.5	-6.5
84	2.8	164	12917	84	2.8	170.5	-6.5
85	2.83	164.5	12849	85	2.83	170.5	-6
86	2.87	164	12784	86	2.87	170.5	-6.5
87	2.9	164.5	12722	87	2.9	170	-5.5
88	2.93	164.5	12664	88	2.93	170.5	-6
89	2.97	164.5	12607	89	2.97	170.5	-6
90	3	165	12554	90	3	170	-5

B.8. Results model 8

Table B.8: Values of the parameters in model 8.

Dfin [mm]	zeta	k_conv [W/m^2K}	tmelt_T0=773 [s]	tmelt_T0=973 [s]	delta_tmelt [s]
50.0	1.4	16188	159	149	-10
48.3	1.45	15802	158.5	150	-8.5
46.7	1.5	15497	159	151.5	-7.5
45.2	1.55	15251	159.5	152	-7.5
43.8	1.6	15050	160.5	152.5	-8
42.4	1.65	14885	160	153.5	-6.5
41.2	1.7	14748	160	154	-6
40.0	1.75	14633	160	155	-5
38.9	1.8	14537	159.5	155	-4.5
37.8	1.85	14455	160	155.5	-4.5
36.8	1.9	14385	160	156	-4
35.9	1.95	14326	160	157	-3
35.0	2	14275	160.5	157	-3.5
34.1	2.05	14232	160.5	158	-2.5
33.3	2.1	14195	160.5	158.5	-2
32.6	2.15	14163	161	158.5	-2.5
31.8	2.2	14136	161.5	158.5	-3
31.1	2.25	14113	161	159	-2
30.4	2.3	14093	161.5	159.5	-2
29.8	2.35	14077	161.5	160	-1.5
29.2	2.4	14063	162	160	-2
28.6	2.45	14052	162	160.5	-1.5
28.0	2.5	14044	162.5	161.5	-1
27.5	2.55	14037	163	161	-2
26.9	2.6	14032	163	161	-2
26.4	2.65	14029	163	161.5	-1.5
25.9	2.7	14027	162.5	161.5	-1
25.5	2.75	14027	163	161.5	-1.5
25.0	2.8	14028	163	162	-1
24.6	2.85	14031	163	162.5	-0.5
24.1	2.9	14035	163.5	162.5	-1
23.7	2.95	14040	163.5	162.5	-1
23.3	3	14047	163.5	162.5	-1

C

Graphs

C.1. Mesh refinement

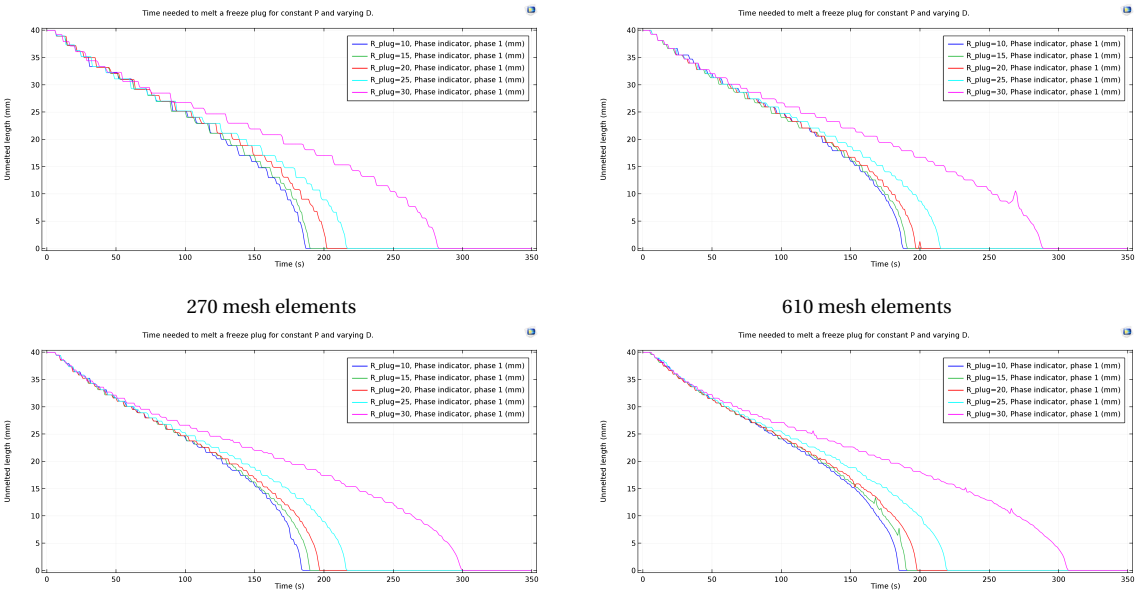

270 mesh elements

610 mesh elements

930 mesh elements

1730 mesh elements

Figure C.1: Melting time for geometry with constant P and varying D using a physics controlled meshes. P is taken to be 70 mm.

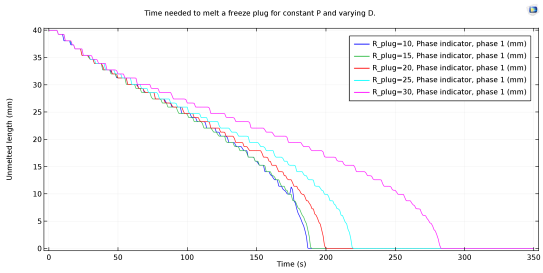

270 mesh elements

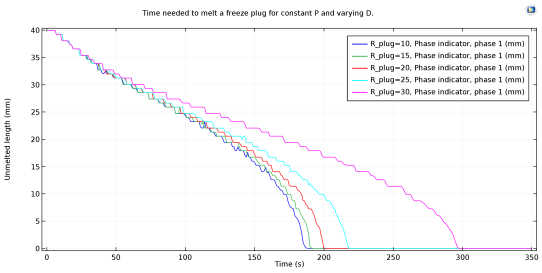

610 mesh elements

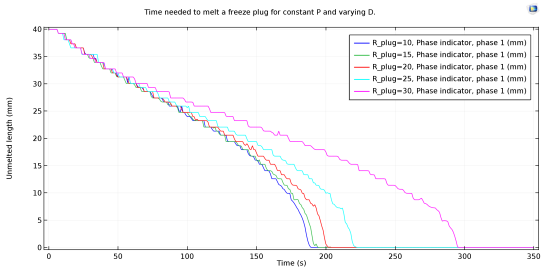

950 mesh elements

Figure C.2: Melting time for geometry with constant P and varying D using a horizontally refined user controlled mesh. P is taken to be 70 mm.

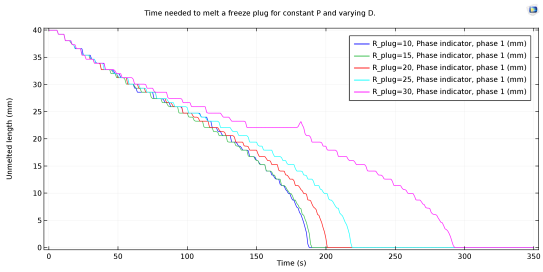

270 mesh elements

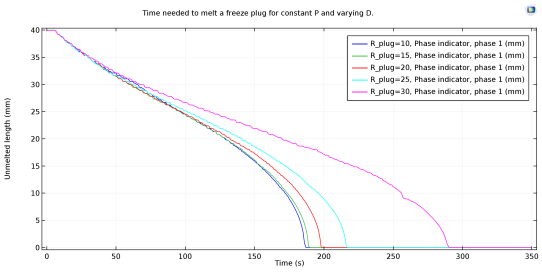

610 mesh elements

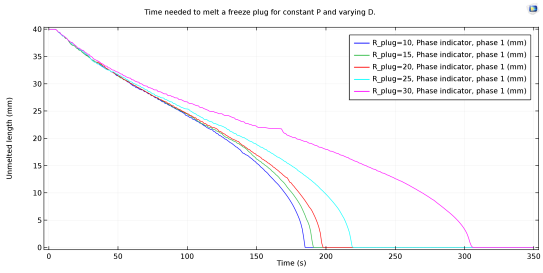

930 elements

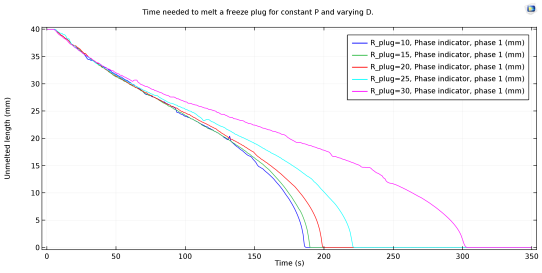

1300 mesh elements

Figure C.3: Melting time for geometry with constant P and varying D using a vertically refined user controlled mesh. P is taken to be 70 mm.

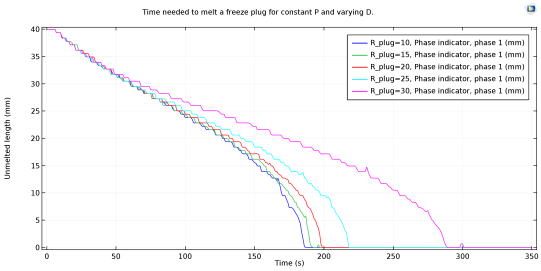

270 mesh elements

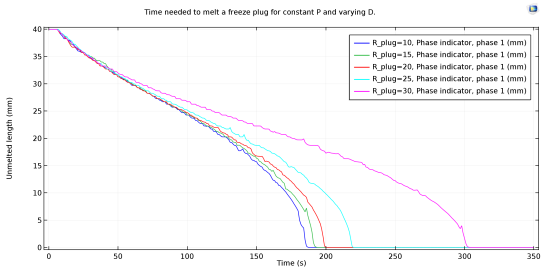

630 mesh elements

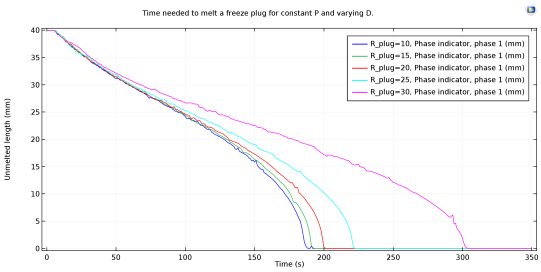

930 mesh elements

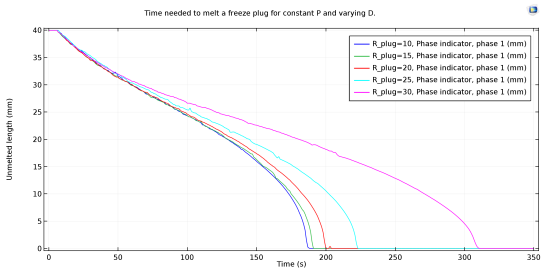

1300 mesh elements

Figure C.4: Melting time for geometry with constant P and varying D using a vertically refined user controlled mesh where a horizontal distribution is included. P is taken to be 70 mm.